

POLITECNICO DI TORINO

Collegio di Ingegneria Chimica e dei Materiali

**Master of Science Course
in Materials Engineering**

Master of Science Thesis

**Innovative microstructured optical fibers as
waveguides for the infrared region**



Tutors

prof. Daniel Milanese

prof. Axel Schülzgen

Candidate

Matteo Facciano

March 2018

*Dedicated to my beloved family and special
friends, which have been always by my side
and are a constant source of inspiration*

Contents

Abstract in Italian	i
1 Introduction	1
1.1 History, background and main applications of optical fibers.....	1
1.2 Research topic, goals and thesis structure.....	3
2 Tellurite glasses	5
2.1 Overview of tellurite glasses, structures and features.....	5
2.2 Photonic applications, state of the art.....	7
2.3 TeO ₂ -ZnO-Na ₂ O (TZN) glass fibers.....	8
3 Optical fibers fabrication	9
3.1 Glass tubes preparation.....	11
3.2 Stack and draw method for microstructured fibers.....	13
3.3 Results and discussion.....	24
4 Characterization	27
4.1 Thermo-mechanical and mechanical properties.....	27
4.1.1 DSC – Differential Scanning Calorimetry.....	27
4.1.2 Dilatometry.....	30
4.1.3 Viscosity.....	30
4.1.4 Hardness.....	32
4.2 Refractive index measurement.....	34
4.3 FTIR Spectroscopy.....	37
4.4 Results and discussion.....	40
5 Conclusions	43
6 Appendix	45
6.1 CVD and materials used.....	45
6.2 DSC curve.....	49
6.3 FTIR spectrum.....	50
7 List of symbols and abbreviations	51

"Innovative microstructured optical fibers as waveguides for the infrared region"

Candidato: Matteo Facciano

Relatore: prof. Daniel Milanese

Introduzione ed obiettivi del lavoro

Il campo delle fibre ottiche è attualmente un ramo della fisica che sta vivendo un periodo di grande sviluppo tecnologico e scientifico. Nel mondo di oggi, infatti, le telecomunicazioni hanno assunto un ruolo di primo piano, richiamando ingenti investimenti. Inoltre, tali dispositivi trovano applicazione anche in altri importanti settori, tra cui sensoristica, illuminazione, trasmissione di potenza, industria biomedica e militare, imaging e automotive.

La funzione primaria delle fibre ottiche è la propagazione della luce con la minor attenuazione possibile del segnale. Per fare ciò, tipicamente si sfrutta il fenomeno della riflessione interna totale (TIR), che permette di confinare il percorso della luce interamente all'interno del materiale. Tale situazione, però, si verifica solo se determinate circostanze vengono rispettate:

- la radiazione elettromagnetica deve muoversi da un materiale a maggior indice di rifrazione verso uno ad indice di rifrazione inferiore;
- l'angolo d'incidenza deve essere maggiore di un certo angolo critico, come rappresentato in Figura 1.

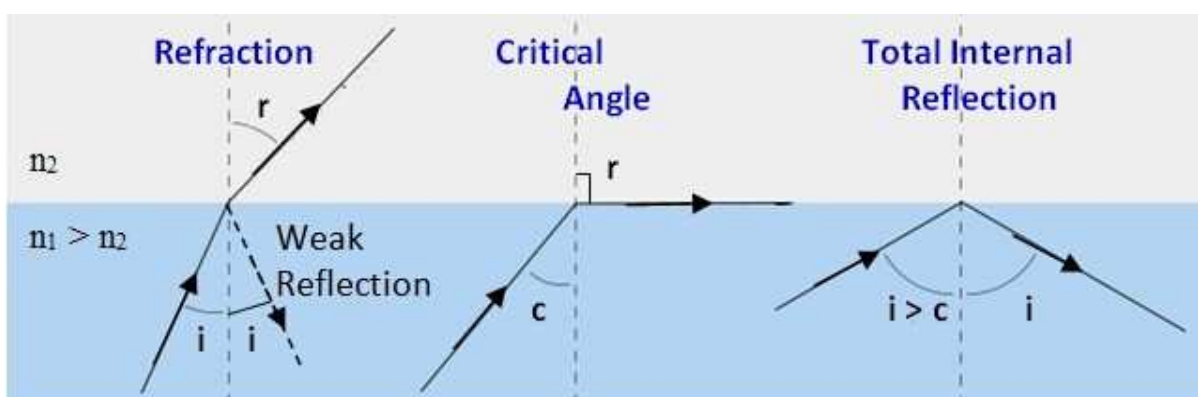


Figura (1). Schematizzazione dei tre possibili comportamenti che il raggio luminoso può assumere all'interfaccia tra due materiali aventi differenti indici di rifrazione n_1 e n_2 . "i" e "c" rappresentano rispettivamente l'angolo d'incidenza e l'angolo critico.

Un altro aspetto importante è quello legato all'architettura delle fibre. La struttura più comune ed utilizzata è la cosiddetta clad-core, illustrata in Figura 2. È composta da una regione centrale chiamata *core* (4-50 μm di diametro), circondata a sua volta da un materiale differente, il

cladding (125 μm di diametro). Infine, vi è inoltre un rivestimento protettivo esterno, detto *jacket* (250 μm di diametro).

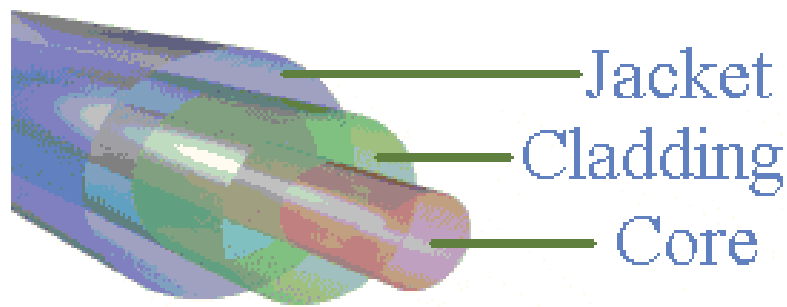


Figura (2). Tipica struttura clad-core per fibre ottiche.

Recentemente, un altro tipo di configurazione sta prendendo piede. Si tratta delle fibre a cristalli fotonici (PCF), fabbricate ponendo particolare attenzione sulla loro microstruttura al fine di conferirne proprietà esclusive. Queste non sono completamente solide, ma anzi possiedono cavità disposte ordinatamente attorno al core, il quale a sua volta può lui stesso essere cavo (Figura 3).

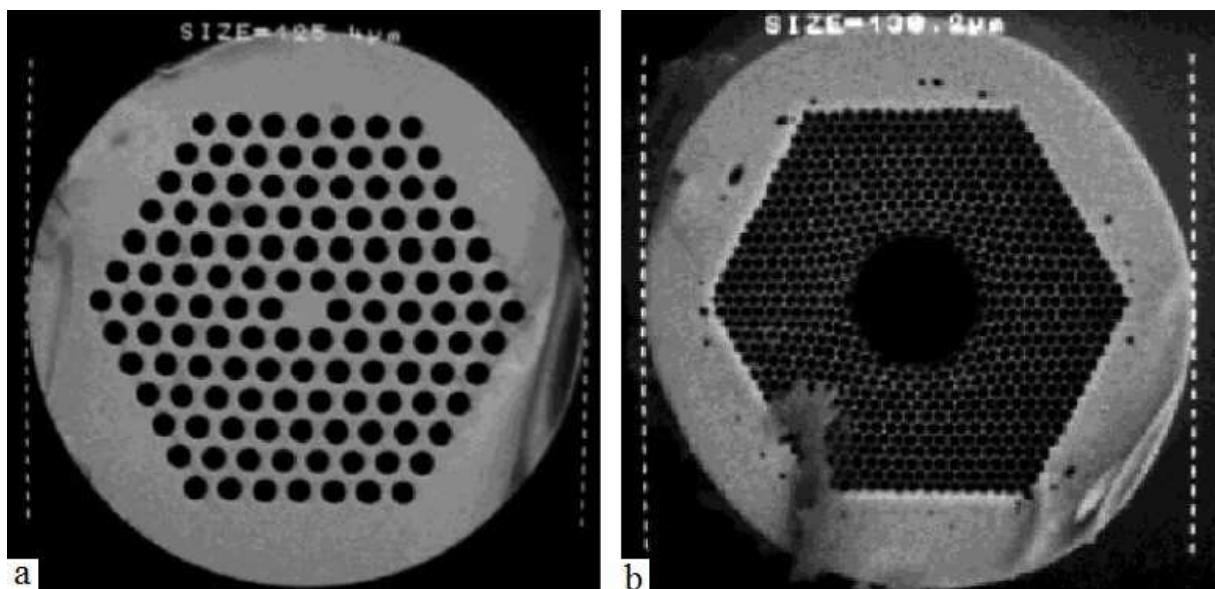


Figura (3). Immagini SEM di una fibra PCF con “dense” core (a) e di una con “hollow” core (b).

Per quanto concerne i materiali utilizzati, la silice ha da sempre rivestito un ruolo esclusivo nel settore delle fibre ottiche grazie al possedimento di caratteristiche ideali: trasparenza alle radiazioni elettromagnetiche, estrema facilità di lavorazione, stabilità termomeccanica e chimica, capacità di ospitare ioni per emissione laser, etc. Tuttavia, essa presenta basse perdite di trasmissione esclusivamente nel vicino infrarosso (1300 – 1700 nm), limitandone l'utilizzo in quella regione dello spettro. Ecco quindi che negli ultimi anni stanno attirando interesse possibili applicazioni a lunghezze d'onda differenti, in particolare nell'infrarosso medio (MIR), ovvero sopra i 2 μm . Alcuni dispositivi di questo tipo sono già stati prodotti, trovando impiego ad esempio in biologia (sensoristica e rilevamento), medicina (diagnostica e chirurgia) e difesa militare (guide ottiche e comunicazioni in spazio libero).

Per le ragioni sopracitate diversi materiali vetrosi alternativi stanno emergendo, tra cui calcogenuri (trasmissione fino a 20 μm), fluorati (trasmissione fino a 2.7 μm) e telluriti (trasmissione fino a 6 μm). In particolare, fibre ottiche a base di vetri telluriti stanno trovando

un certo spazio all'interno della comunità scientifica, grazie ad alcune loro proprietà peculiari. Oltre a possedere un'estesa finestra di trasmissione che va dal VIS fino al MIR, questo materiale presenta un'accettabile optical damage threshold, bassa fotosensibilità e perdite intrinseche piuttosto contenute. Inoltre, la sua stabilità nei confronti di fenomeni di cristallizzazione consente di sperimentare diverse strategie di filatura in fibra, permettendo la fabbricazione di un'ampia varietà di strutture. Un'ulteriore elemento chiave risiede nell'elevato indice di rifrazione, pari a 1.8 – 2.2 a seconda della composizione. La solubilità verso ioni di terre rare è altresì notevole (circa 50 volte maggiore rispetto alla silice), dando ulteriori opportunità di ingegnerizzare le caratteristiche finali del materiale.

L'obiettivo principale del presente lavoro di tesi, dunque, è stato quello di indagare proprietà, processabilità e possibili applicazioni come fibra ottica PCF di un particolare tipo di vetro tellurito, mantenendo un approccio basato sulla scienza e tecnologia dei materiali. Il materiale in questione è detto TZN, la cui composizione in percentuale molare è la seguente: 75% TeO₂, 15% ZnO, 10% Na₂O.

Partendo dalla produzione del vetro TZN presso il Politecnico di Torino, lo studio è proseguito presso The University of Central Florida con la sua caratterizzazione ed il tentativo di adoperarlo nella fabbricazione di fibre ottiche microstrutturate opportunamente progettate.

Metodologie utilizzate

Avendo a che fare con un materiale relativamente nuovo nel campo della fotonica, durante la sua lavorazione è stato necessario ideare nuove metodologie ed adattare su misura alcune di quelle usualmente utilizzate per la fabbricazione di fibre ottiche a base silice.

Il primo passo è stato quello di realizzare le preforme della composizione desiderata. Il processo è consistito nella fusione della miscela di ossidi di partenza all'interno di un crogiolo di platino e successivo riempimento di uno stampo in cui far avvenire la solidificazione. I precursori di partenza sono stati: diossido di tellurio (TeO₂), ossido di zinco (ZnO) e carbonato di sodio (Na₂CO₃). La miscela, avente un peso iniziale di 80 g, ha poi subito il seguente trattamento termico:

- riscaldamento da temperatura ambiente fino a 750 °C ad una velocità di 10 °C/min;
- permanenza a 750 °C per 3 h;
- raffreddamento da 750 °C a 690 °C ad una velocità di 10 °C/min;
- permanenza a 690 °C per 1 h.

In seguito, poiché le preforme erano richieste di forma tubolare, il materiale fuso è stato processato tramite *rotational casting*. Tale tecnica ha previsto la colata ed il raffreddamento in uno stampo di ottone, preriscaldato ad una temperatura attorno alla T_g del composto e messo in rotazione ad una velocità di 3000 rpm. Il tubo così ottenuto ha poi immediatamente subito un trattamento di ricottura ad una temperatura di 280 °C per 5 h, al fine di conseguire una riduzione degli stress residui. Ottenere un vetro con sufficiente resistenza meccanica e basso rischio di frattura è essenziale per una buona riuscita degli stadi successivi. Un altro aspetto molto importante riguarda il livello di purezza raggiunto, che dipende principalmente dalla qualità dei precursori. Particolare attenzione dev'essere altresì posta nel limitare il più possibile la presenza di gruppi ossidrilici ed altre impurezze. A questo proposito, l'intero processo è stato effettuato all'interno di un ambiente ultra-clean. La preparazione della miscela di polveri è stata eseguita in una dry-box avente un'atmosfera di azoto, mentre la fase di fusione è avvenuta in una glove-box.

Complessivamente, due tubi di vetro tellurito TZN sono stati prodotti. Uno di essi è riportato in Figura 4.

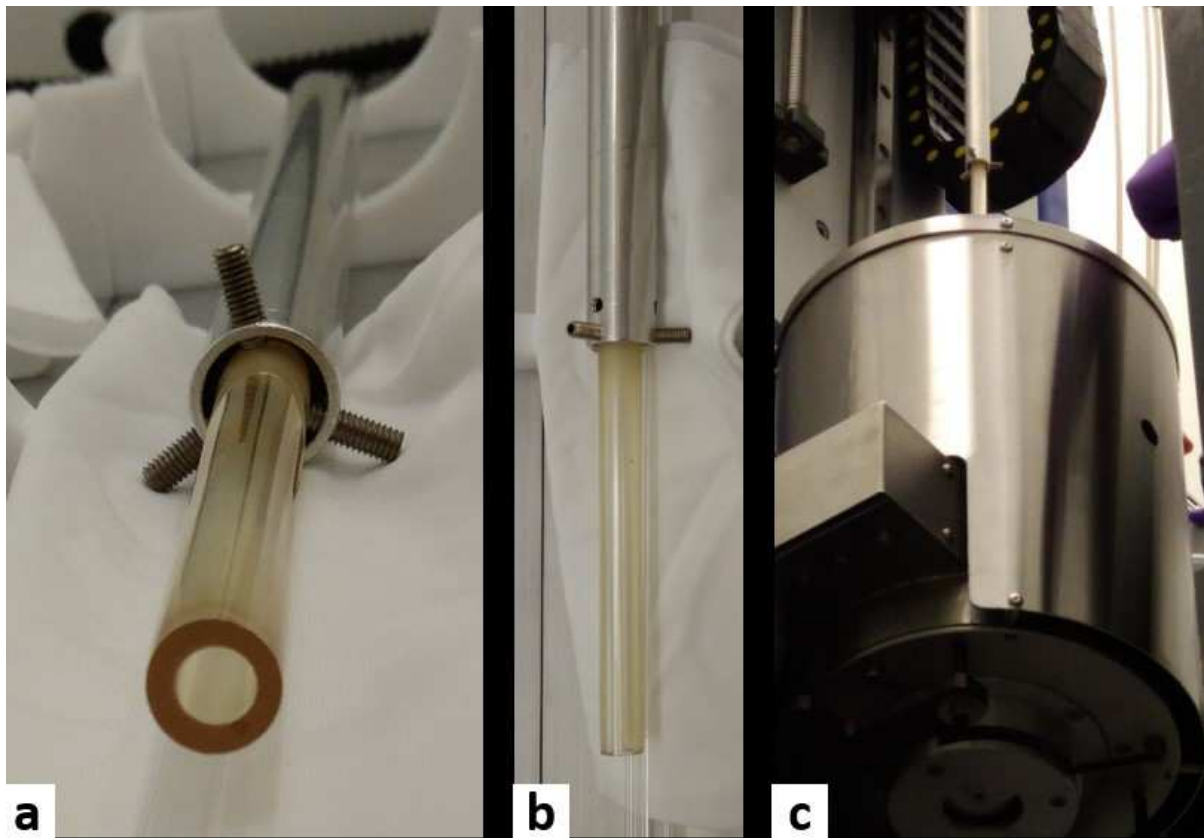


Figura (4). Immagini che mostrano uno dei due tubi realizzati via rotational casting. Il componente è stato collocato all'interno di un tubo di lega di alluminio 6061 e fissato ad esso con tre viti (a, b) per poter essere posizionato verticalmente nella torre di filatura (c).

A questo punto, per la fabbricazione di fibre a cristalli fotonici è stata impiegata la tecnica dello *stack-and-draw*. Essa consiste nel creare macroscopicamente la struttura desiderata accatastando manualmente capillari e/o barre del materiale prescelto all'interno di un tubo, che funge da jacket. Tale preforma viene poi consolidata e filata fino ad ottenere una preforma intermedia di dimensioni molto più ridotte (solitamente 1 – 2 mm di diametro), come mostrato in Figura 5. Quest'ultima, può essere infine filata nuovamente per realizzare le fibre di dimensione e microstruttura volute.

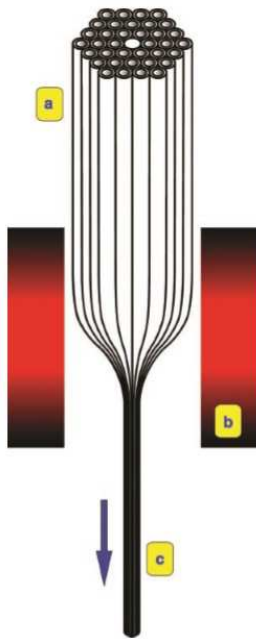


Figura (5). Illustrazione della tecnica dello stack-and-draw. La preforma macroscopica avente la struttura desiderata (a) è posizionata nella torre di filatura (b) e filata al fine di ottenere una preforma intermedia (c).

In generale, il procedimento cambia leggermente di volta in volta in base alle caratteristiche del dispositivo che si vuole ottenere. Nello specifico, per la realizzazione di fibre TZN si è operato come segue:

- uno dei due tubi di partenza è stato sottoposto a filatura con lo scopo di fabbricare capillari della taglia desiderata, da impiegare poi per la creazione della preforma macroscopica;
- i capillari così ottenuti sono stati tagliati in segmenti più corti, assecondando la lunghezza del tubo utilizzato come jacket;
- la geometria della microstruttura scelta è stata realizzata macroscopicamente accatastando opportunamente i segmenti prodotti in precedenza. Due diverse configurazioni (A e B) sono state create, ciascuna occupante circa metà della lunghezza del tubo. La “configurazione A” può essere osservata in Figura 6, mentre per la “configurazione B” si rimanda alla lettura del Chapter 3;
- la preforma macroscopica, dopo essere stata consolidata, è stata trasferita alla torre di filatura e processata per essere ridotta a preforma intermedia.

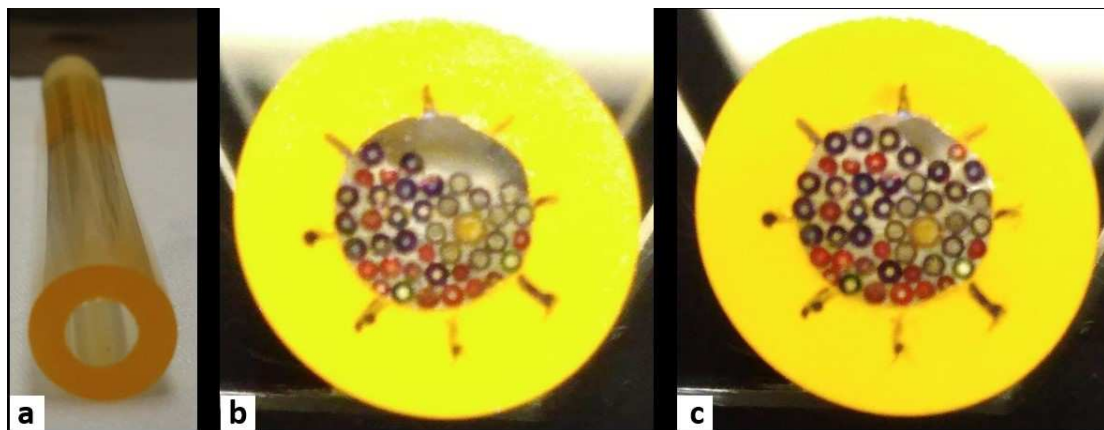


Figura (6). Diversi stadi della fase di assemblaggio. Il tubo (a), impiegato come jacket, è stato gradualmente riempito con capillari (b, c).

Caratterizzazione

Le metodologie di caratterizzazione compiute sul vetro TZN hanno permesso l'investigazione di diverse sue proprietà ed una migliore comprensione del suo possibile comportamento. Tutti i campioni utilizzati nelle misurazioni sono stati acquisiti dalla filatura del primo tubo (Figura 4). Precisamente, dopo aver collezionato i residui che presentavano dimensioni adeguate, quest'ultimi sono stati lavorati affinché soddisfacessero i requisiti delle varie strumentazioni. A seguire vengono presentate e descritte le apparecchiature che sono state utilizzate.

Calorimetria differenziale a scansione (DSC)

Per questa misura è stato impiegato un TA instruments DSC Q10 (Figura 7). Esso è composto da una camera contenente due identici contenitori portacampione, che possono essere riscaldati tramite due radiatori indipendenti. Il materiale da esaminare è posto in uno dei recipienti, mentre l'altro, vuoto, serve come riferimento. I due contenitori vengono poi scaldati alla medesima velocità (stesso $\Delta T/\Delta t$). Ciò genera una differenza di flusso termico ($\Delta Q/\Delta t$) tra le due scatole, in quanto una di esse è caratterizzata da maggiore capacità termica per via della presenza del campione. In questo modo, rilevando tale differenza si possono mettere in relazione flusso di calore e temperatura. Riportando i dati in un grafico (Figura 8) è possibile individuare le temperature caratteristiche del composto, in corrispondenza delle quali si verifica un brusco cambio di flusso termico.



Figura (7). TA instruments DSC Q10 utilizzato per la calorimetria differenziale a scansione.

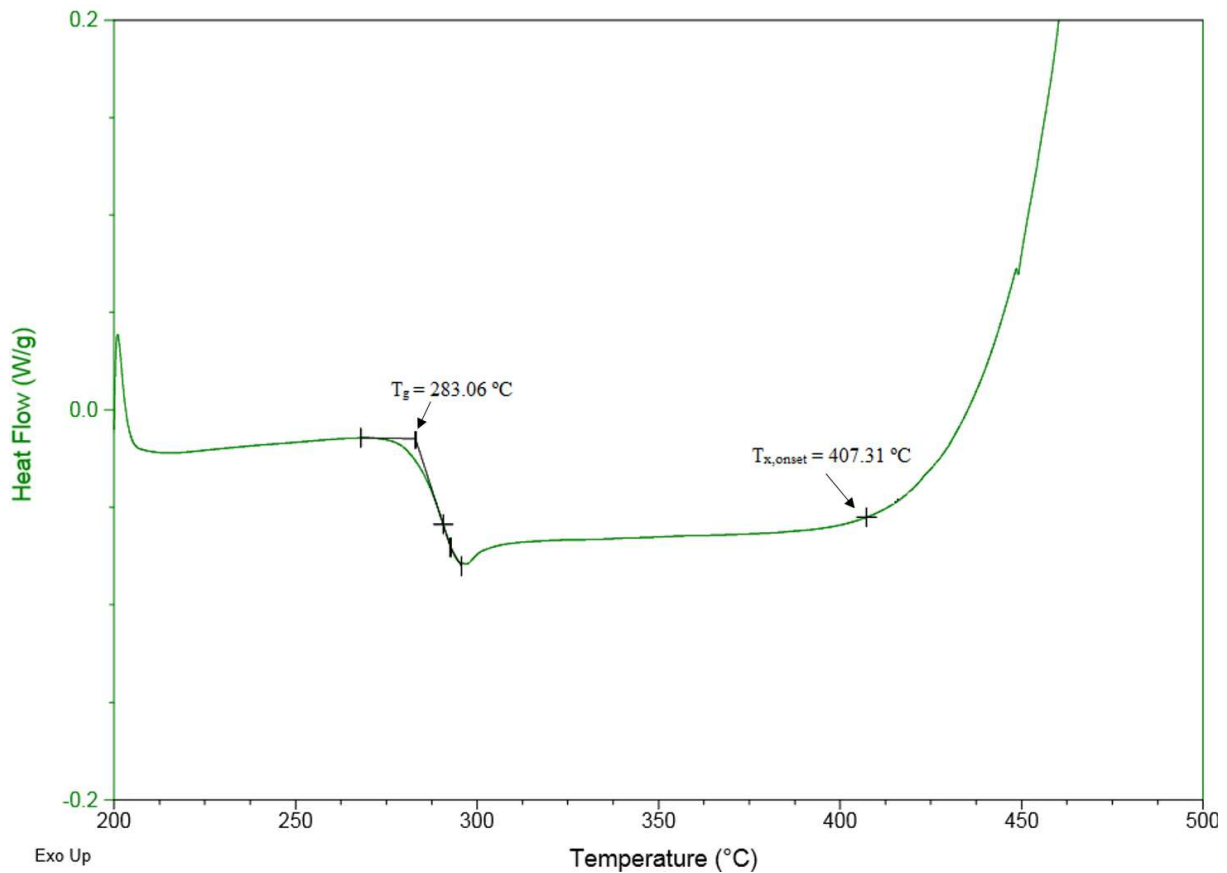


Figura (8). Spettro DSC eseguito sul vetro TZN. Le temperature caratteristiche individuate sono la temperatura di transizione vetrosa T_g e la temperatura di inizio cristallizzazione $T_{x,onset}$.

Microdurezza Vickers

Per il test di microdurezza Vickers ci si è serviti di un Shimadzu DUH-211S (Figura 9). La prova consiste nell'applicare sul campione un carico statico di compressione per un certo tempo, allo scopo di creare un'indentazione sulla sua superficie. La durezza è poi determinata dal rapporto tra la forza applicata e l'area dell'impronta. L'indentatore in questione è una punta di diamante piramidale a base quadrata avente un angolo pari a 136° , che conferisce all'impronta una geometria ben definita (Figura 10). In questo modo, il valore di durezza può essere calcolato tramite la formula seguente:

$$HV = \frac{F}{A} = \frac{F}{\frac{d^2}{2 \sin(136^\circ/2)}} = 1.8544 \frac{F}{d^2}, \quad (1)$$

dove F è la forza applicata (in kgf) e d è la lunghezza della diagonale dell'impronta (in mm).

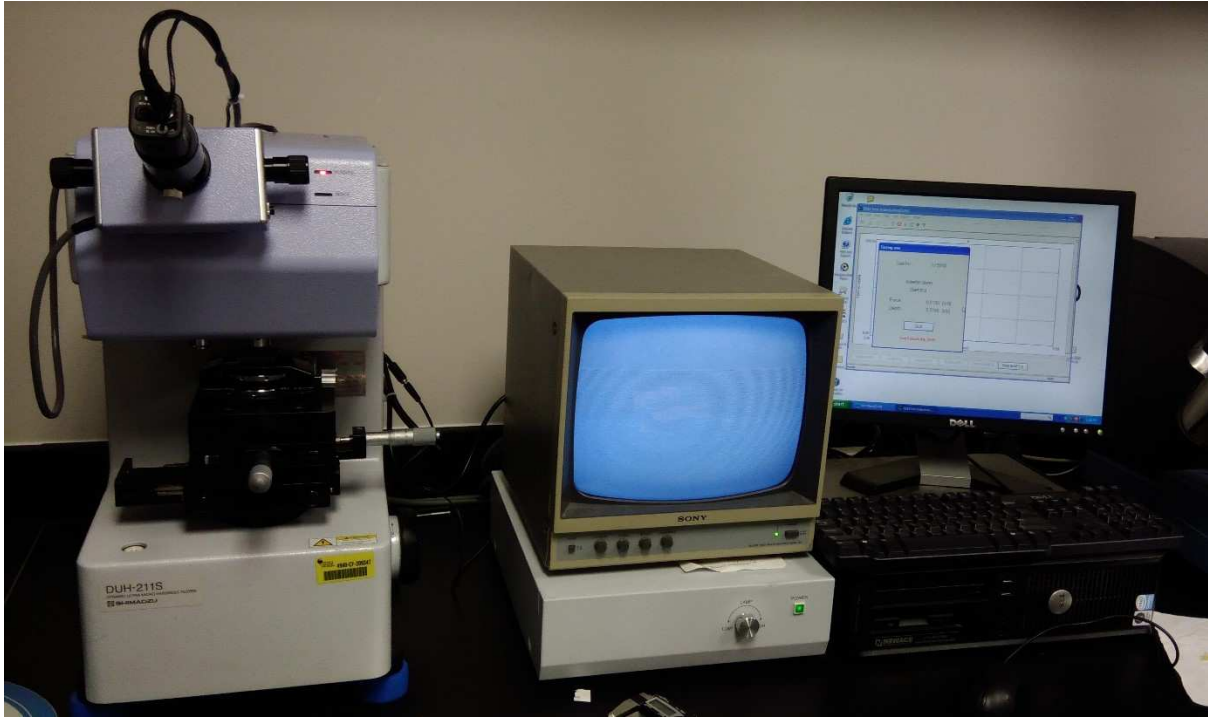


Figura (9). Shimadzu DUH-211S utilizzato per il test di microdurezza Vickers.

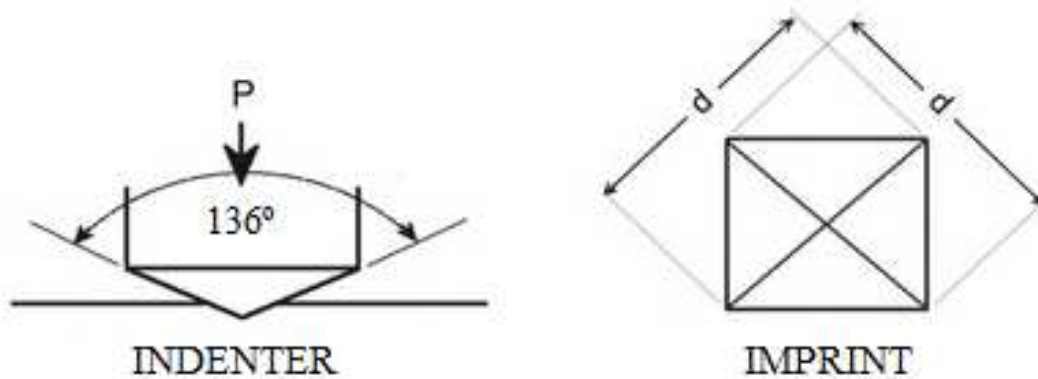


Figura (10). Schema raffigurante l'indentatore Vickers (sinistra) e la geometria dell'impronta generata sulla superficie testata (destra).

Prism coupler

Il "prism coupling" è un metodo che consente di misurare l'indice di rifrazione di un materiale, il cui principio di funzionamento è basato sul setup sperimentale di Figura 11. Il campione, in forma di substrato, è posto a contatto tramite pistone con un prisma avente elevato indice di rifrazione. Una luce laser di lunghezza d'onda predefinita è lanciata attraverso il prisma e, a causa della TIR, viene riflessa alla base di esso. Un photodetector posto sul lato opposto rileva l'intensità della luce rifratta. L'angolo di riflessione θ può essere superiore o inferiore all'angolo critico θ_c , a seconda dell'inclinazione del raggio incidente. L'angolo di incidenza viene quindi fatto variare fino a quando il fascio laser non penetra nel substrato generando una drastica caduta d'intensità del segnale rilevato. Tale condizione dipende dal θ_c dell'interfaccia prisma/substrato, da n del prisma e da n del substrato. Poiché quest'ultima grandezza è l'unica incognita, può essere dunque calcolata.

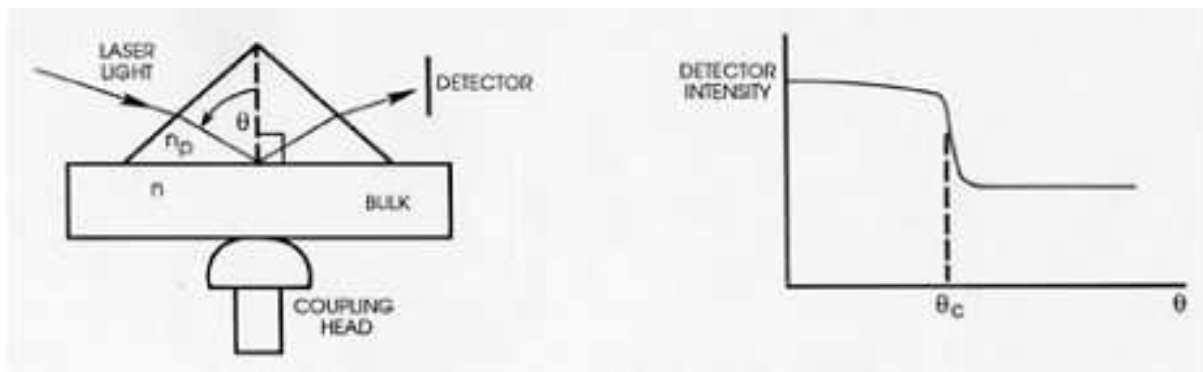


Figura (11). Schema raffigurante il setup sperimentale (sinistra) ed il grafico Angolo vs. Intensità (destra).

Per questa misura è stato impiegato un TA instruments DSC Q10 (Figura 12), equipaggiato con un prisma di GaP ed una sorgente laser a 0.98 μm .

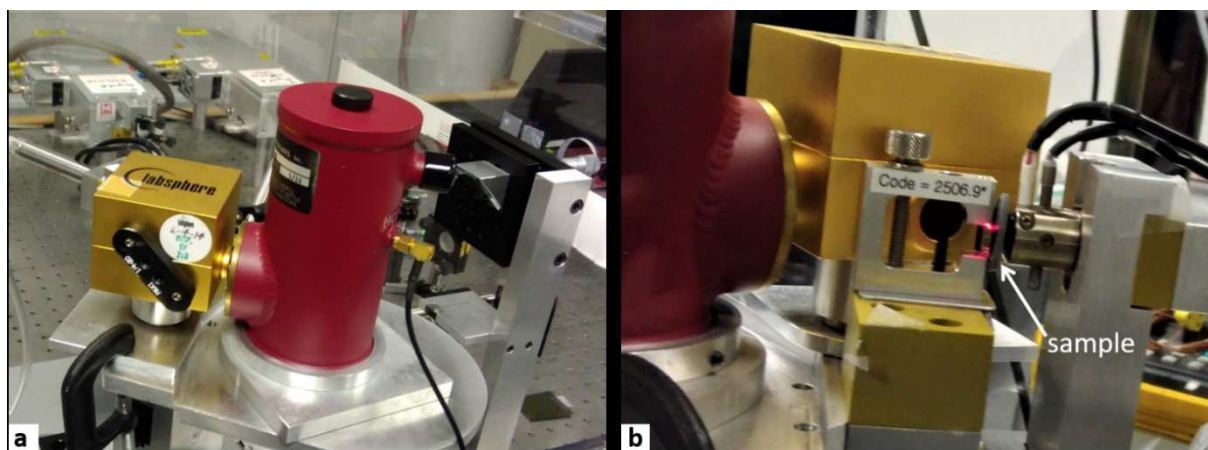


Figura (12). Metriton Model 2010/M Prism Coupler utilizzato per la misura dell'indice di rifrazione (a). Il campione è collocato tra il prisma ed il pistone (b).

Spettroscopia FTIR

Per la spettroscopia infrarossa è stato impiegato un Thermo Scientific Nicolet iS5 FTIR Spectrometer (Figura 13), in grado di misurare lo spettro di trasmissione nell'intervallo tra 400 cm^{-1} e 7000 cm^{-1} . Il suo principale vantaggio rispetto agli spettrofotometri tradizionali a dispersione risiede nella capacità di raggruppare tutte le lunghezze d'onda simultaneamente. Infatti, invece di lavorare con una luce monocromatica, questo strumento fa uso di un fascio contenente l'intero range di frequenze da misurare. Una volta raccolti i dati riguardanti la quantità di luce assorbita dal campione, il fascio viene modificato ed una nuova misura viene effettuata a combinazione di frequenze differente. Questa procedura viene reiterata fino ad ottenere tutte le informazioni necessarie. A quel punto, i dati vengono processati da un calcolatore che applica la trasformata di Fourier per estrarre lo spettro di trasmissione (Figura 14). Per ogni lunghezza d'onda d'interesse, la trasmittanza è calcolata tramite l'equazione seguente:

$$T = I/I_0, \quad (2)$$

dove I_0 è l'intensità iniziale del raggio di luce ed I l'intensità rilevata dopo il passaggio attraverso il campione.



Figura (13). Thermo Scientific Nicolet iS5 FTIR Spectrometer utilizzato per l'analisi FTIR.

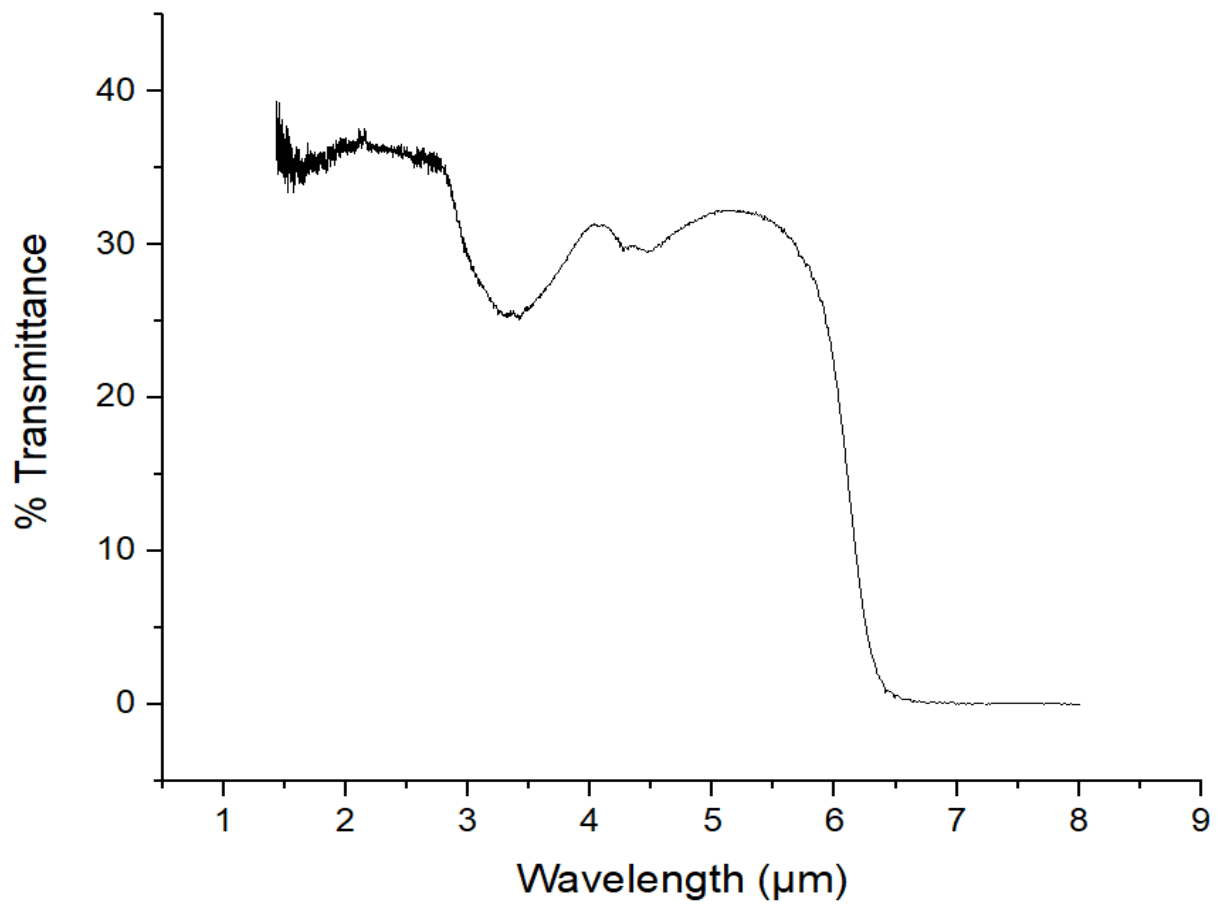


Figura (14). Spettro FTIR del vetro TZN nell'intervallo di lunghezze d'onda tra 1.4 µm e 8 µm.

Discussione dei risultati

Il vetro tellurito è un materiale molto fragile e dev'essere maneggiato con estrema cautela. Questo aspetto aumenta le difficoltà che si possono incontrare durante il processo di fabbricazione di fibre ottiche. Inoltre, dal momento che le sue proprietà fisiche differiscono molto da quelle della silice, durante lo stack-and-draw si sono verificate alcune complicanze che hanno reso necessaria l'ideazione di strategie alternative. In particolare, i maggiori problemi affrontati sono stati:

- ottenere un buon controllo sulla variazione di viscosità con la temperatura e, di conseguenza, sull'intero processo di filatura. A differenza della silice, infatti, il vetro tellurito può essere lavorato in un intervallo di temperatura molto ristretto, all'interno del quale la sua viscosità può cambiare significativamente anche a seguito di una variazione di pochi gradi. Tutto ciò ha portato all'ottenimento di capillari di diametro molto variabile;
- progettare e realizzare la microstruttura utilizzando capillari molto eterogenei in termini di diametro (sia interno che esterno). Questa situazione non ideale non ha reso possibile, per quanto concerne la "configurazione A", posizionare il core esattamente nel centro, come mostrato in Figura 15. È importante rimarcare come la decentralizzazione del core non comprometta affatto la propagazione della luce, in quanto ciò che realmente conta è la geometria attorno ad esso. A questo proposito, per ottenere un adeguato confinamento, si è provveduto a formare nel suo intorno un anello di 7 capillari, impiegando quelli più dimensionalmente costanti a disposizione;
- l'impossibilità, una volta terminata la preforma macroscopica, di consolidarne la struttura servendosi di una semplice fiamma all'ossidrogeno. In alternativa, si è dovuto utilizzare una fornace tubolare, che ha reso la procedura più complicata e dispendiosa in termini di tempo. Oltretutto, durante questo passaggio la parte iniziale della preforma ha subito dei danneggiamenti;
- l'esigenza di fabbricare appositamente un tubo in lega di alluminio che consentisse l'applicazione del vuoto durante la fase di filatura. Tale componente era necessario, in quanto la strategia adottata anteriormente era risultata inadeguata ed aveva portato al danneggiamento della parte terminale della preforma. Ciò è risultato poi determinante sull'esito dello stadio di filatura successivo.



Figura (15). Vista frontale della "configurazione A" che mette in evidenza la posizione del core e del primo anello di 7 capillari che lo circonda.

Nonostante tutte le contromisure adottate, durante la filatura finale si è verificato un cedimento strutturale della preforma che ne ha provocato la caduta e la derivante frammentazione. Dunque, non è stato possibile fabbricare le PCFs desiderate.

Conseguentemente, uno spazio considerevole del Chapter 3 è dedicato all'analisi delle possibili cause ed alla presentazione di plausibili strategie alternative volte a evitare il ripresentarsi delle medesime complicanze.

Per quanto riguarda le caratterizzazioni, esse hanno permesso di indagare ed analizzare le proprietà d'interesse del vetro TZN. I valori ottenuti per differenti proprietà fisiche, misurati direttamente o ricavati dalla letteratura scientifica, sono riportati in Tabella 1.

Tabella (1). Valori di proprietà fisiche del vetro TZN, tra cui composizione chimica, temperatura di transizione vetrosa T_g , temperatura di inizio cristallizzazione $T_{x,onset}$, stabilità termica ΔT , coefficiente di dilatazione termica α , microdurezza Vickers HV, indice di rifrazione n a $0.98 \mu\text{m}$.

Composizione Chimica (% molare)	75%TeO₂-15%ZnO-10%Na₂O
$T_g \pm 2 \text{ }^\circ\text{C}$	283 $^\circ\text{C}$
$T_{x,onset} \pm 2 \text{ }^\circ\text{C}$	407 $^\circ\text{C}$
ΔT	124 $^\circ\text{C}$
α (25 $^\circ\text{C}$ - 250 $^\circ\text{C}$)	$18.8 \times 10^{-6} \text{ }^\circ\text{C}^{-1}$
microdurezza Vickers $\pm 9 \text{ HV}$	323 HV
n a $0.98 \mu\text{m} \pm 0.0002$	2.0008

Dalla calorimetria differenziale a scansione è emersa un'adeguata stabilità nei confronti della devettrificazione. Questo consente di portare avanti processi di filatura senza doversi preoccupare di possibili fenomeni di cristallizzazione.

A causa della mancanza di un campione adeguato e dell'impossibilità di realizzarne uno, il coefficiente di espansione termica è stato ricavato dalla letteratura scientifica invece che sperimentalmente.

Lo stesso vale per la viscosità, con la differenza che in questo caso non è stato possibile dedurre dei risultati accurati da altre pubblicazioni. Sono stati trovati solamente alcuni valori appartenente ad una composizione affine. Dato che si tratta di una proprietà cruciale per il processo di filatura, una sua misura diretta sarebbe necessaria.

Il test di durezza ha confermato l'elevata fragilità del materiale, il quale risulta propenso a subire danneggiamento alla minima sollecitazione applicata.

La misura dell'indice di rifrazione ha portato all'esito che ci si attendeva, sebbene si riferisca ad un'unica lunghezza d'onda ($0.98 \mu\text{m}$). Sarebbe utile ripetere l'esperimento usando differenti fonti laser in modo da indagare come questo valore cambi al variare della lunghezza d'onda.

Siccome lo spettro di trasmissione è risultato essere ampio, con condizioni ideali fino a quasi $3 \mu\text{m}$, ci sono buone probabilità che una fibra ottica TZN possa essere testata con successo come sorgente di supercontinuo. Ulteriori miglioramenti nella riduzione del contenuto di gruppi ossidrilici potrebbe permettere di estendere la generazione di supercontinuo, teoricamente fino a $6 \mu\text{m}$.

Conclusione

I vetri telluriti possiedono diverse proprietà che rivelano la possibilità di portare avanti ricerca scientifica e sviluppo tecnologico. Con questo elaborato si è voluto presentare un quadro generale delle caratteristiche peculiari che li contraddistinguono, ponendo particolare enfasi sul comportamento ottico e termomeccanico.

La caratterizzazione ha reso possibile analizzare il vetro TZN della composizione selezionata. Calorimetria differenziale a scansione, durezza, metodo del prism coupling e spettroscopia FTIR sono stati gli strumenti utilizzati. In aggiunta, la ricerca bibliografica ha permesso di dedurre valori plausibili di viscosità e coefficiente di espansione termica.

Una buona parte del lavoro è stata interamente dedicata alla progettazione e fabbricazione di fibre a cristalli fotonici TZN attraverso la tecnica dello stack-and-draw. L'inaspettato esito negativo dello stadio finale di filatura in fibra ha precluso la possibilità di ottenere e caratterizzare tali componenti. L'attenzione è stata quindi rivolta all'indagine delle cause plausibili dell'insuccesso.

Complessivamente, l'attività sperimentale condotta è stata altresì utile per acquisire esperienza e dimestichezza nella lavorazione del materiale. Questo aspetto può fare la differenza qualora venisse intrapreso un nuovo tentativo di fabbricazione di fibre TZN.

1 Introduction

1.1 History, background and main applications of optical fibers

Nowadays we witness how technology is evolving very rapidly in many fields, heading our society towards what it begins to be identified as “The Fourth Industrial Revolution”. In such a world that changes every day faster and where physical, digital and biological spheres are all interconnected, new areas of opportunities, as well as challenges, are arising.

Fiber optics is undoubtedly a noteworthy part of physics that is observing important developments and investments, largely due to its vital importance for communication systems. In global telecommunications technologies, indeed, optical fibers represent a primary component, related to an industry that generates over 1 billion dollars in annual revenue [1]. The success of the Internet is strictly associated to fiber communications, too, leading to the intent of developing even faster fiber networks. But not only that, since optical fibers find employment in many other fields such as sensing, power transmission, illumination, imaging, biomedical industry, military, automotive and more.

Sensing is one of the most widespread applications among the ones listed above and therefore deserves further attention. Fiber probes are utilized for the detection of variations in temperature, pressure, strain, voltage and other environmental conditions. Furthermore, another crucial analysis that can be carried out is real-time monitoring of chemical reactions. This technique turns out to be crucial when dealing with special samples hard to handle, because its flexibility allows to overcome the difficulties encountered with usual spectrometers. In addition to their versatility, fiber optic probes are known to be very sensitive as well as having immunity to electromagnetic interference, small size, lightweight, large bandwidth and ease in implementing multiplexed or distributed sensors [2].

The primary function of fiber optics is to propagate light along their length with minimum attenuation of the signal, typically due to Total Internal Reflection (TIR) phenomenon. TIR takes place when:

- the light ray goes from a material with higher refractive index to a material with lower refractive index;
- the angle of incidence is greater than the critical angle, as can be seen in Figure 1.1.

This principle allows to confine light inside the material and make it travel along the fiber.

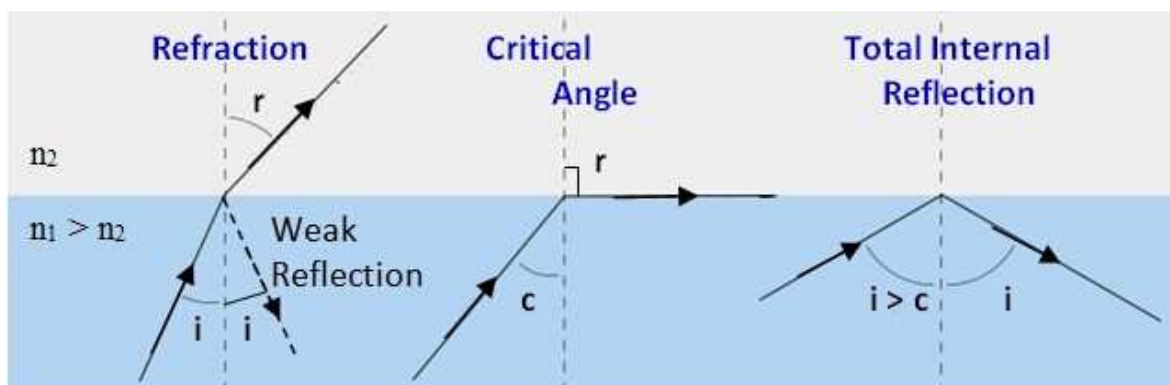


Figure 1.1. Schematization of the possible behaviors of a light ray at the interface between two media having different optical densities, with “i” as incident angle and “c” as critical angle (figure retrieved from <http://www.excelatphysics.com> with modifications).

The feasibility of light-guiding was demonstrated as far back as 1841 by Daniel Colladon, a 38-year-old professor at the University of Geneva; but it was only in the 1950s that optical fibers started to be developed [3]. Since then, several breakthroughs were made. In 1966, Kao and Hockmann, at the Standard Telecommunications Laboratories in England, proved that the major transmission attenuation in glass fibers was due to the presence of impurities rather than an intrinsic material property, suggesting them as a practical medium for telecommunications if the attenuation could be reduced to below 20 dB/km. That goal was soon obtained in 1970, by researchers at Corning Glass Works which drew a preform produced by Outside Vapor Phase Oxidation (OVPO) [3]. Nowadays, numerous optical fibers with attenuation less than 0.5 dB/km at certain wavelengths have been fabricated.

Glass, composed of different elements depending on the application, is the major material utilized in fiber manufacture, due to the possibility of obtaining low-loss propagation of optical frequencies, far less than in metallic waveguides [1]. The most widely used is silica glass, which presents a refractive index of approximately 1.5. Hence, silica optical fibers are thin cables of glass able to transmit light at around two-thirds of the speed of light in vacuum.

This material has many features ideal for photonic applications: transparent to electromagnetic radiations, obtainable homogeneously in many shapes, dimensions and chemical compositions, capable of hosting laser-active ions, temperature-stable and chemically stable against several chemical agents and corrosive environments, abundant and inexpensive (especially for large-scale productions).

Besides silica, other glasses are currently studied and employed to make fibers, as will be discussed in more detail in the next section.

On the other hand, for low speed and short distance applications, also polymer optical fibers (POFs) can be fabricated, typically using PMMA as the core and fluorinated polymers as the cladding (Figure 1.2). They normally have much higher losses than glass fibers, but they are relatively inexpensive [4].

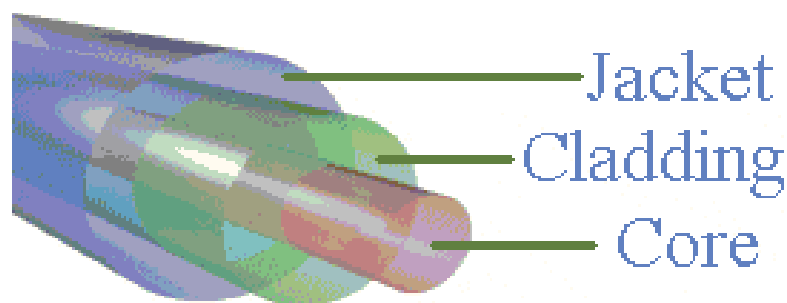


Figure 1.2. Clad-core structure of optical fibers (figure retrieved from <http://www.pef.uni-lj.si/eprolab/comlab>).

Figure 1.2 shows the most common structure of optical fibers, which is called clad-core structure. It is made of a central portion, the core (typically 4-50 μm of outer diameter), enveloped by the cladding (125 μm), which has a lower refractive index. Finally, an external coating called jacket (250 μm) covers and protects the inner parts.

Since inside a fiber light can propagate in different ways and velocities, two types are possible: single-mode and multi-mode. A single-mode fiber only supports one propagation mode, whereas a multi-mode fiber allows more than one mode of light to propagate at the same time. Recently, another class of optical fibers is gaining attention, i. e. photonic crystal fibers (PCF). They are fabricated with a special focus on their microstructure, which is strongly controlled in order to give them unique propagation properties (Figure 1.3).

Besides solid-core PCFs, even hollow-core PCFs can be realized. The latter ones are designed to guide light in an empty or gas-filled hollow core. These features seem to have encouraging prospects for the production of new fibers that could overcome the limitations of conventional ones, although some progress is still necessary [5].

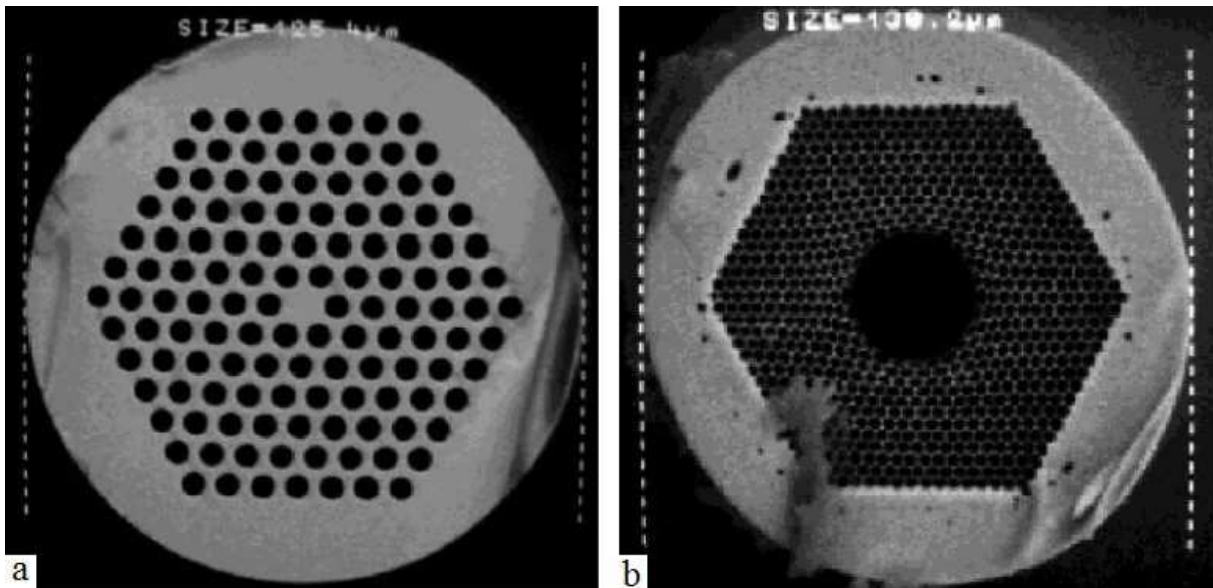


Figure 1.3. SEM images of a single dense core PCF fiber (a) and a hollow core PCF fiber (b) (figure retrieved from [6] with modifications).

1.2 Research topic, goals and thesis structure

Fiber optics research has always been mainly focused on the development of silica fibers, involving also new optical technologies and innovative fiber designs (e.g. microstructured and dispersion-shifted). However, due to their low loss and dispersion in the near-IR range of wavelengths (1300 – 1700 nm), most utilizations have been exclusively in that spectrum region. As a result, in the last few years new applications at wavelengths different from those of the third telecommunication window (1550 nm) are becoming attractive, especially in the mid-infrared (MIR), which refers to wavelengths above 2 μm . Nowadays we can find uses in biological issues (sensing and detection/imaging), medical (diagnostic and surgical) and defense (optical guidance and free space communications) to mention some [7].

Nevertheless, since silica transmits only until 2 μm , different materials are emerging as good candidates for making glass optical fibers, such as fluorides (transmission up to $\sim 2.7 \mu\text{m}$), chalcogenides (transmission up to $\sim 20 \mu\text{m}$) and tellurites (transmission up to $\sim 6 \mu\text{m}$) [7]. Within this vast and variegated world of fiber optics, then, tellurite glass optical fibers are earning interest among the scientific community in the last few years, thanks to some peculiar properties.

Indeed, in addition to an extended transmission window that goes from the VIS to the MIR, this material presents acceptable optical damage threshold, little photosensitivity and quite low intrinsic loss if compared to chalcogenides [7]. On the other hand, its crystallization stability leads to several possibilities of fiber drawing, allowing the fabrication of a wide variety of structures. Another key feature consists in a refractive index usually in the range of 1.8-2 depending on the exact composition, which can be adjusted introducing other ions. It is important to emphasize that the solubility of rare earth ions is particularly high (~ 50 times higher than silica), permitting to modify, along with the introduction of other glass

modifiers/formers, its dispersion profile, emission cross-section and nonlinear coefficients [7, 8].

The promising characteristics of tellurite glasses listed above motivated the realization of this study, whose main goal was to employ this material to successfully design, fabricate and characterize microstructured optical fibers to use as waveguides for the IR region.

The work has been carried out at CREOL, The University of Central Florida College of Optics & Photonics, in collaboration with Politecnico di Torino, where tellurite glass tubes were fabricated.

Thesis structure

Chapter 1 presents the world of fiber optics in its entirety and the challenges scientists are facing nowadays, putting special attention to the topic developed in this work.

Chapter 2 is totally dedicated to tellurite glasses and their main features. A significant part is focused on the opportunities this material has in the field of photonics; in particular, TZN glass fibers, which are the ones under investigation in this study, are taken into specific consideration.

Chapter 3 reports and describes in detail the techniques used in the attempt of fabricating TZN fibers, from tubes preparation to the drawing of microstructured fibers.

Chapter 4 shows and investigates specific properties of the glass, taking advantage of several methods of characterization, including spectroscopy, refractive index measurement and thermo-mechanical analysis.

Chapter 5 sums up all the considerations emerged in the previous chapters and discusses homogeneously the results obtained in order to draw some conclusions.

Chapter 6 is a section that contains additional data useful to better understand the subjects presented in this study.

Chapter 7 is a list of abbreviations and symbols used in the body of the disquisition, providing a definition for each of them.

2 Tellurite glasses

2.1 Overview of tellurite glasses, structures and features

A glass is defined as an amorphous material, since it does not possess a crystal structure. The lack of long-range order gives to this class of materials some unique features, including isotropy of many properties, thermodynamic metastability and presence of a glass transition temperature (range) instead of an exact melting temperature. The existence of a metastable state is related to the fabrication method: it is obtained as a result of a quick cooling process from the liquid phase, which inhibits the crystallization and leads to a very disorganized spatial arrangement similar to the liquid from which it originates. Evidently, the phase just described is unstable and a nucleation of crystals can begin whenever the thermodynamic and kinetic conditions are favorable. This last consideration, along with the fact that viscosity is continuously varying with temperature, are the issues of most concern during fiber optics fabrication, as will be discussed in more detail in Chapter 4.

On the other hand, glasses are very flexible in terms of chemical composition, which usually consists of several elements and can be modified in order to obtain the desired properties. In general, three categories of components can be found in the structure, classified according to their function. The main constituent is the *glass former*, a substance that can vitrify and, thus, build the amorphous network; silica (SiO_2), boron trioxide (B_2O_3), germanium dioxide (GeO_2) and phosphorus pentoxide (P_2O_5) are examples of materials that assume that role. Oxides such as sodium oxide (Na_2O), potassium oxide (K_2O) and calcium oxide (CaO) are instead called *modifiers*. They are not able to vitrify, but they lightly bond to the former provoking the interruption of its glass network. Because of that, the features of the material change significantly, including its characteristic temperatures. Indeed, since the network is weakened, a decrease of viscosity occurs, facilitating glass workability. Finally, there are components such as alumina (Al_2O_3) or titanium dioxide (TiO_2) which, in little amount, can substitute the glass former and take part in the amorphous network; they are called *intermediates* and they also cause properties modification.

Regarding the material used within this work, tellurium oxide (TeO_2) performs the role of glass former, whereas zinc oxide (ZnO) and sodium oxide (Na_2O) act as modifiers. Admittedly, tellurium oxide was initially known just as intermediate and it was only in the 1980's that researchers were able to effectively use it as glass former; the key was to introduce modifiers that could break some TeO_2 bonds and open the network [9]. Indeed, Te-O is a strong covalent bond and pure tellurite usually crystallizes at cooling, having a TeO_4 trigonal bi-pyramid (tbp) as fundamental structural unit. The glassy state, instead, is composed of distorted versions of the structural element mentioned above, since the insertion of modifiers causes a weakening of Te-O bonds. Thus, the latter become longer and two other sub-units come into the picture: a TeO_{3+1} distorted trigonal bi-pyramid and a TeO_3 trigonal pyramid (tp) [9, 10]. The three structures are illustrated in Figure 2.1

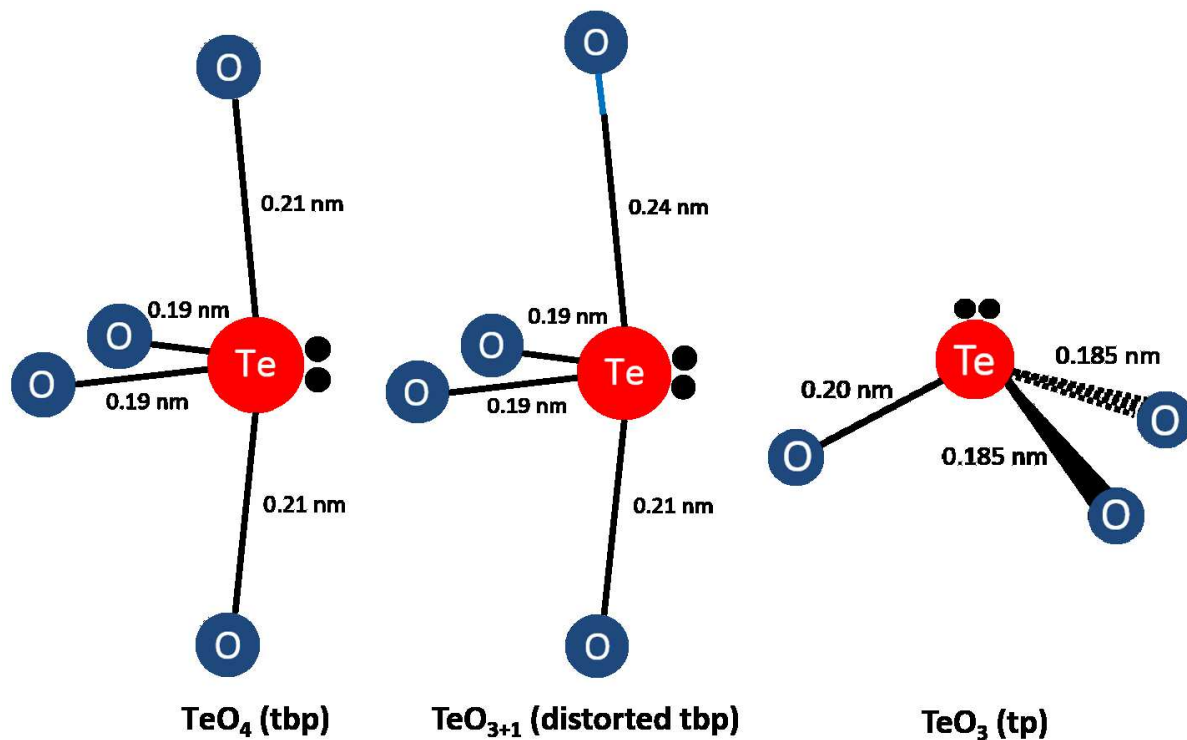


Figure 2.1. Structural representation of Te-O subunits that form TeO₂ glasses, including bond lengths in nm: TeO₄ trigonal bi-pyramidal (left), TeO₃₊₁ distorted trigonal bi-pyramidal (center) and TeO₃ trigonal pyramidal (right).

According to [10], TeO₄ tbp has bond lengths of 0.21 nm for the axial oxygens and 0.19 nm for the equatorial oxygens, whereas the TeO₃₊₁ elongated one can be from 0.22 nm to 0.26 nm long and Te-O bonds belonging to TeO₃ tp extend from 0.185 nm to 0.20 nm.

Some peculiar features that bring out tellurite glasses are:

- broad range of transmission that goes from 0.4 μm to 5 μm. It is approximately twice as wide as the one belonging to silica glass (0.2 - 2.5 μm), making it a promising material for both visible and mid-IR applications [11];
- low hygroscopy, namely low inclination to attract and absorb water molecules. This aspect helps to improve the resistance to environmental degradation, which is much higher compared to other competitors for mid-IR such as fluoride glasses. However, its solubility in water is two orders of magnitude greater than the one of chalcogenide glasses [9];
- stability against crystallization within the temperature range suitable for fiber fabrication. This characteristic will be further analyzed in Subsection 4.1.1;
- high refractive index, between 1.8 and 2.3 depending on chemical composition. This fact is crucial for many cutting-edge optical properties including photon emission, where high values of n are preferred [9];
- high solubility of rare-earth elements, up to $22 \cdot 10^{20} \text{ cm}^{-3}$, which allows to tailor peculiar features such as luminescence, fluorescence and high linear refractive index. Thanks to that, tellurite glasses are also attractive as possible active fibers for fiber lasers and fiber amplifiers [11].

Other general properties are gathered and compared to silica in Table 2.1.

Table 2.1. Comparison between TeO₂ and SiO₂ of physical and optical properties. Some values might slightly differ depending on exact chemical composition [11].

<i>Properties</i>	<i>TeO₂</i>	<i>SiO₂</i>
<u>Physical properties</u>		
Density	5.5 g/cm ³	2.2 g/cm ³
Young's modulus	50.7 GPa	73.1 GPa
Poisson ratio	0.23	0.17
Melting point	732 °C	1600 °C
Glass transition temperature	280 – 480 °C	1000 °C
Coefficient of thermal expansion	12 - 17 · 10 ⁻⁶ °C ⁻¹	0.55 · 10 ⁻⁶ °C ⁻¹
Dielectric constant	13 – 35	4.0
Predominant bonding	Covalent	Covalent
<u>Optical properties</u>		
Linear refractive index	1.9 – 2.3	1.46
Abbe number	10 – 20	80
Transmission range	0.4 – 5 μm	0.2 – 2.5 μm
Phonon energy	780 cm ⁻¹	1100 cm ⁻¹
Band gap	3 eV	10 eV
Theoretical minimum fiber loss and loss minimum wavelength	20 dB · km ⁻¹ (2.8 – 3 μm)	0.2 dB · km ⁻¹ (1.55 μm)

2.2 Photonic applications, state of the art

The first research publication on tellurite glass goes back to 1956, when G. Barady proved the feasibility of making a stable TeO₂ glass by using lithium oxide (Li₂O) as modifier. However, its prospective properties for photonic applications only emerged in the 1990's, when fiber amplifiers were fabricated by E. Vogel at Bell Labs; they were doped with erbium and praseodymium and showed significant gain. Since then, many optical amplifiers with high gain have been manufactured, as well as microstructured optical fibers for supercontinuum generation and microlenses for biomedical applications and telecommunication. To date, this material has also been successfully employed to produce photonic nanowires, planar waveguides, channel waveguides and optical switches [9].

Indeed, in the last few years some noteworthy achievements in fabricating tellurite glass devices have been attained. A selection of them is presented as follows.

M.P. Belançon et al. obtained a broadband near-infrared emission source based on a tellurite-tungstate glass doped with Pr³⁺, ideal for optical amplification [11]. L. Tong et al. were able to manufacture tellurite glass nanowires that showed encouraging properties for the realization of nanophotonic devices and circuits. The method used consisted in directly draw the wires from bulk glass [12]. Starting from a 75TeO₂-2GeO₂-10Na₂O-12ZnO-1Er₂O₃ (molar ratio) tellurite glass doped with Er³⁺, V. A. G. Rivera succeeded in realizing planar waveguides using an Ag⁺→Na⁺ ion exchange technique [13]. Finally, by M. Liao et al. was reported a nonlinear tellurite MOF that exhibits supercontinuum generation when pumped with a continuous wave laser [14].

2.3 $\text{TeO}_2\text{-ZnO-Na}_2\text{O}$ (TZN) glass fibers

In recent years tellurite glasses are increasingly succeeding in the field of fiber optics, as evidenced by the growing number of articles published (175 in 2017 compared to just 5 in 1987) [9]. Several chemical compositions are now widespread, including $\text{TeO}_2\text{-PbO}$, $\text{TeO}_2\text{-ZnO-La}_2\text{O}_3\text{-Na}_2\text{O}$, $\text{TeO}_2\text{-WO}_3\text{-La}_2\text{O}_3$, fluorotellurites and many more [8].

Among them, TZN glasses are also frequently employed. The acronym indicates the presence of tellurium dioxide (T), zinc oxide (Z) and sodium oxide (N). These three substances can be clearly mixed in different ratios. Common proportions contemplate a molar % content of TeO_2 between 70% and 85%. By way of example, a standard composition is 75% TeO_2 -20% ZnO -5% Na_2O (TZN75).

TZN group was identified as one of the best tellurite glass compositions in terms of thermal stability within the fabrication range. It also offers ample opportunities to select a pair of compositions with admissible thermal mismatch in view of stable core-cladding fiber structures [9].

Coefficient of thermal expansion, glass transition temperature, crystallization temperature, phonon energy and refractive index are just some of the properties that can be modulated. It is well known, for instance, that higher content of ZnO causes a decrease of both interatomic distance (rise in density) and refractive index, whereas T_g increases. The introduction of Na_2O , instead, decreases T_g , since it shows worse integration inside the glass network compared to zinc oxide [11].

TZN family has attracted attention principally for supercontinuum generation and laser applications in the MIR, also because its capability of hosting large quantities of rare earth ions permits to customize specific optical properties. The main limitation of TZN-based devices lies with their thermomechanical stability, which is restricted by the combination of elevated coefficient of thermal expansion ($18 - 20 \cdot 10^{-6} \text{ }^\circ\text{C}^{-1}$) and low glass transition temperature (around 300 $^\circ\text{C}$). This implies that, under certain circumstances, possible damage due to overheating or thermally induced stresses can take place (low laser induced damage threshold). Besides that, the good processability through fiber drawing of this kind of glasses offers further ways of development, since several microstructured designs can be fabricated, each one giving a unique optical behavior to the fiber. The first example of TZN photonic crystal fiber for MIR nonlinear applications is dated 2006 by T. Delmonte et al. [15]. They used a 75 TeO_2 -20 ZnO -5 Na_2O single-mode PCF characterized by a triangular solid core with a diameter of 2.6 μm . The spectral range was between 0.9 μm and 2.5 μm and a pump source at 1.5 μm was used. The main strategies currently employed for PCFs fabrication will be discussed in detail in the next chapter.

3 Optical fibers fabrication

In order to obtain high quality fibers is crucial to use high-purity materials, since the presence of impurities such as copper, iron, vanadium, and hydroxyl groups, can significantly alter the optical properties of the system.

Additionally, whenever two different materials are put in contact, some important matching requirements must be satisfied. In this specific case:

- the refractive index of the core must be greater than the refractive index of the cladding, in order that TIR can occur;
- the coefficient of thermal expansion (CTE) of the two materials should be almost the same to minimize tensions at the interface induced during solidification;
- for similar reasons, also the glass transition temperature (T_g) of the two materials must have values close to each other;
- the fiber drawing must be realized at a temperature well below the crystallization temperature (T_x) of the glasses [4].

Almost every fabrication process starts with the realization of a so-called *preform*, a replica on a larger scale of the fiber structure, either by *rod-in-tube* technique or *chemical vapor deposition* (CVD).

In the first method, as its name suggests, the core, in the form of a rod, is inserted into a cladding tube (Figure 3.1). Traditional fabrication methods imply melt quenching for rod and tubes [16].

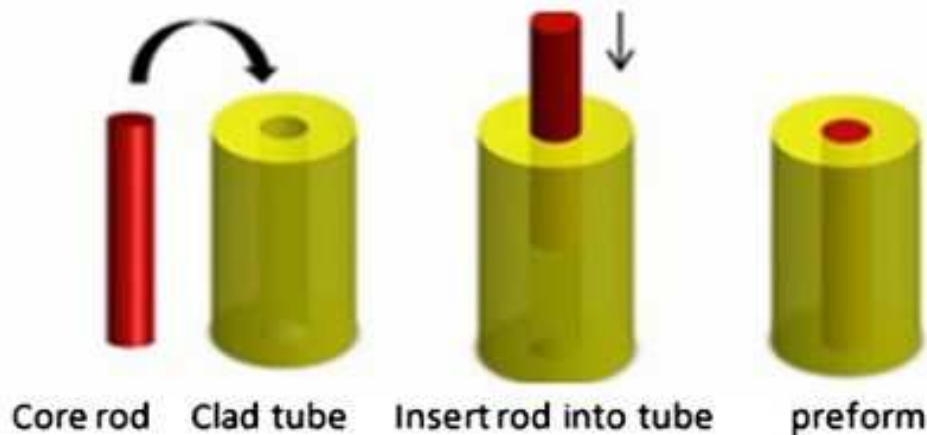


Figure 3.1. Schematic illustration of rod-in-tube technique (figure retrieved from [17] with modifications).

However, most of preforms are nowadays realized by CVD, a well-developed technology that permits to obtain low loss fibers (<0.5 dB/km), ideal for long-range applications; it is considered the optimum in terms of costs for mass production.

Among the variety of CVD methods, the *modified chemical vapor deposition* (MCVD) is the most common. It was first reported by MacChesney et al. in the 1970s for the realization of silica telecom fibers [18]. In this case, the preform is obtained in consequence of vapor phase deposition of silica and some dopants that derive from chemical precursors. High temperature oxidation is the principal type of reaction, which takes place inside a rotating silica glass tube. The latter is warmed up by an external oxyhydrogen heat source that goes back and forth. The stream of high purity gas-phase reagents can include SiCl_4 , GeCl_4 , BCl_3 , BBr_3 , PCl_3 , POCl_3 ,

SF₆, CF₄ and CCl₂F₂, along with oxygen [18, 19]. Glassy particles are formed as a result of the reaction and produce a fine film of soot on the inner hot zone, which is then sintered into a glass layer. The procedure is repeated the number of times required to get a certain amount of material, that is formed layer by layer and whose composition can be changed each time. Thus, it is possible to control the refractive index along the radial direction. Finally, the tube is heated up above its softening temperature and collapsed into a solid preform rod [16, 18]. Figure 3.2 shows a schematic of the process.

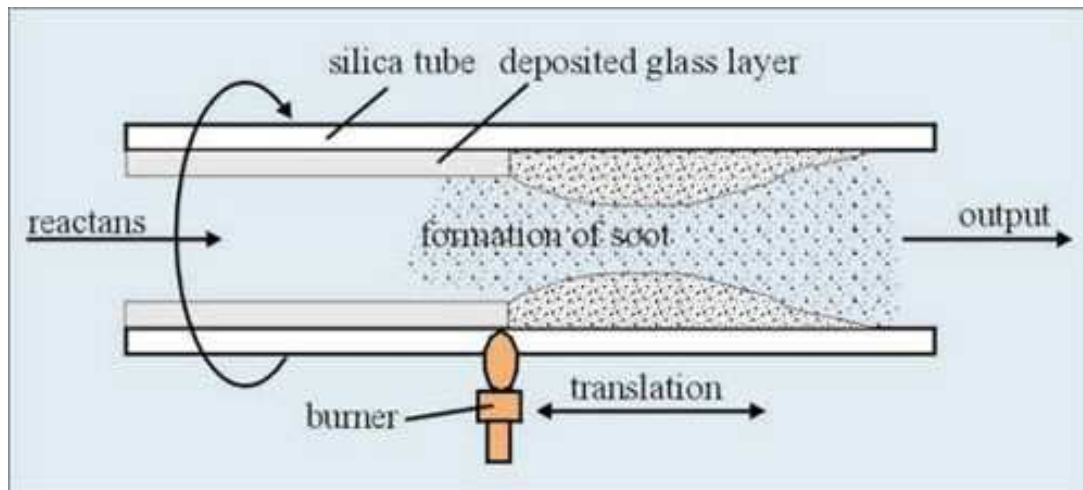


Figure 3.2. Schematic illustration of MCVD method (figure retrieved from <http://csrg.ch.pw.edu.pl>).

Besides MCVD, other vapor deposition methods have been elaborated, including:

- *Outside vapor deposition (OVD)*, whose main difference is that deposition does not occur inside a tube but on the outer surface of a rotating rod (e.g. a glass mandrel). In this case the first material deposited is the core, whereas the cladding is formed afterwards. Then, the central rod is taken away and the hollow preform is put in a furnace to make it collapse into a dense tube; also, a drying gas is injected in order to decrease the hydroxyl content. This process was designed in the early 1970s at Corning Glass Works [16, 20, 21];
- *Vapor phase axial deposition (VAD)*, which is akin to OVD but with a different geometry that allows to perform deposition and consolidation in the same production line. In fact, the rod is constantly pulled away along the axial direction, from the burner to the furnace. Thus, it is possible to fabricate very long fiber preforms. It was proposed for the first time in 1979 at NTT Laboratories, in Japan [16, 20, 22];
- *Plasma chemical vapor deposition (PCVD)*, which works with the same principles of MCVD but uses microwaves to heat the deposition zone (inner part of a tube). The process is more time-consuming but it is extremely accurate [16, 23].

The communal advantages of all these methods are that there is no contamination and high-purity precursors can be employed [18]. Further information about CVD processes and the materials used for vapor deposition can be found in Appendix 6.1.

The next step consists in getting the fiber from the preform. To do that, the preform is positioned vertically in a drawing tower, which is a large equipment in height that includes:

- a mandrel that holds the preform vertically;
- a tube furnace that gives the thermal energy necessary to soften the glass and reach the required viscosity to allow for drawing the optical fiber;

- a laser micrometer that controls fiber diameter;
- a system that applies a UV-cure coating of photopolymer around the fiber;
- a dynamometer to measure fiber tension;
- a winding drum to collect the fiber obtained.

The preform, placed at the top of the tower, is heated above its T_g (but below its T_x) and pulled downwards. As a result, a fiber with a controlled diameter comes out from the bottom of the furnace. It is then coated in order to give chemical and mechanical protection and, finally, rolled up around the winding drum. Polyimide, acrylate and silicone are habitual polymers used as coatings [16].

It is important to underline that drawing parameters affect some features of the fiber, especially its diameter and internal stress distribution. The main parameters to deal with are the temperature of the furnace, the preform feeding speed and the rotational speed of the winding drum (pulling speed).

There is also a fabrication method that does not involve a preform, called the *double crucible method*. It is a melting process based on extrusion that allows a direct fiber production, although the greater presence of impurities leads to higher attenuations. Thick optical fibers (250-400 μm of outer diameter) and soft glass fibers are the types more often fabricated with this procedure, but only for short-range applications. The melted core glass is introduced into the inner crucible, which has a central opening, while the melted cladding glass lies on the outer one. The two glasses meet inside the outer crucible so that core and cladding can be drawn together. This technique has the advantage of conforming easily to different materials, but it is not appropriate for ultrapure fibers fabrication [16].

3.1 Glass tubes preparation

Speaking of tellurite glasses the situation is a bit different, given that a gaseous compound of TeO_2 needed for the chemical vapour deposition is intricate to get [17]. Here the method typically used to fabricate the preform consists in melting the precise mixture of oxides inside an inert crucible (usually of platinum), filling a mold and finally cooling down to get the desired shape. Consequently, the level of purity achieved depends on the quality of the initial raw materials. A special attention must also be paid to limiting as much as possible the hydroxyl content, as well as the presence of dust and other impurities. For the reasons just mentioned, the process is carried out in an ultra-clean environment. Moreover, time and temperature should be precisely monitored to impede the development of micro-bubbles, especially during glass melting and pouring.

Since the aim of the study was to fabricate PCFs, for the preform a tubular shape was chosen. The glass tubes preparation was performed at Politecnico di Torino, where two tubes were realized.

The OH content was minimized operating in a dry-box with nitrogen atmosphere during powder mixing and in a glove box during melting. The method used to fabricate the adequate shape was rotational casting, a well-known technique that allows to obtain a smooth inner surface. The best quality is achievable by choosing the right mold preheating parameters, the optimized furnace rotational speed and the appropriate time [17].

The final tubes were fabricated using the following raw materials: tellurium dioxide (TeO_2), zinc oxide (ZnO) and sodium carbonate (Na_2CO_3). The composition chosen was, in molar ratio, 75% TeO_2 , 15% ZnO , 10% Na_2O , since it looks a good prospect for the realization of nonlinear optical fibers.

The initial batch weight for the production of one tube was 80 g. The mixture was melted inside a platinum crucible using the following thermal treatment:

- heating from room temperature to 750 °C at a heating rate of 10 °C/min;
- dwell at 750 °C for 3 h;
- cooling from 750 °C to 690 °C at a cooling rate of 10 °C/min;
- dwell at 690 °C for 1 h.

Then, the molten material was poured and quenched, by rotational casting, into a cylindrical brass mold preheated at a temperature around T_g and at a rotational speed of 3000 rpm. Immediately after, the tube obtained was lastly annealed inside the mold at a temperature of 280 °C for 5 h. The annealing process is very important to reduce residual stresses that form inside the material during the fabrication procedure. Achieving a glass with enough strength and low risk of cracking is essential for further manufacturing steps.

In Figure 3.3 is shown one of the two samples produced, which presents a longitudinal length of 110 mm, an outer diameter of 11.4 mm and an inner diameter of 6.8 mm. The other one had a longitudinal length of 110 mm, an outer diameter of 10.8 mm and an inner diameter of 6 mm. As a final step, they were polished in preparation for fiber drawing.

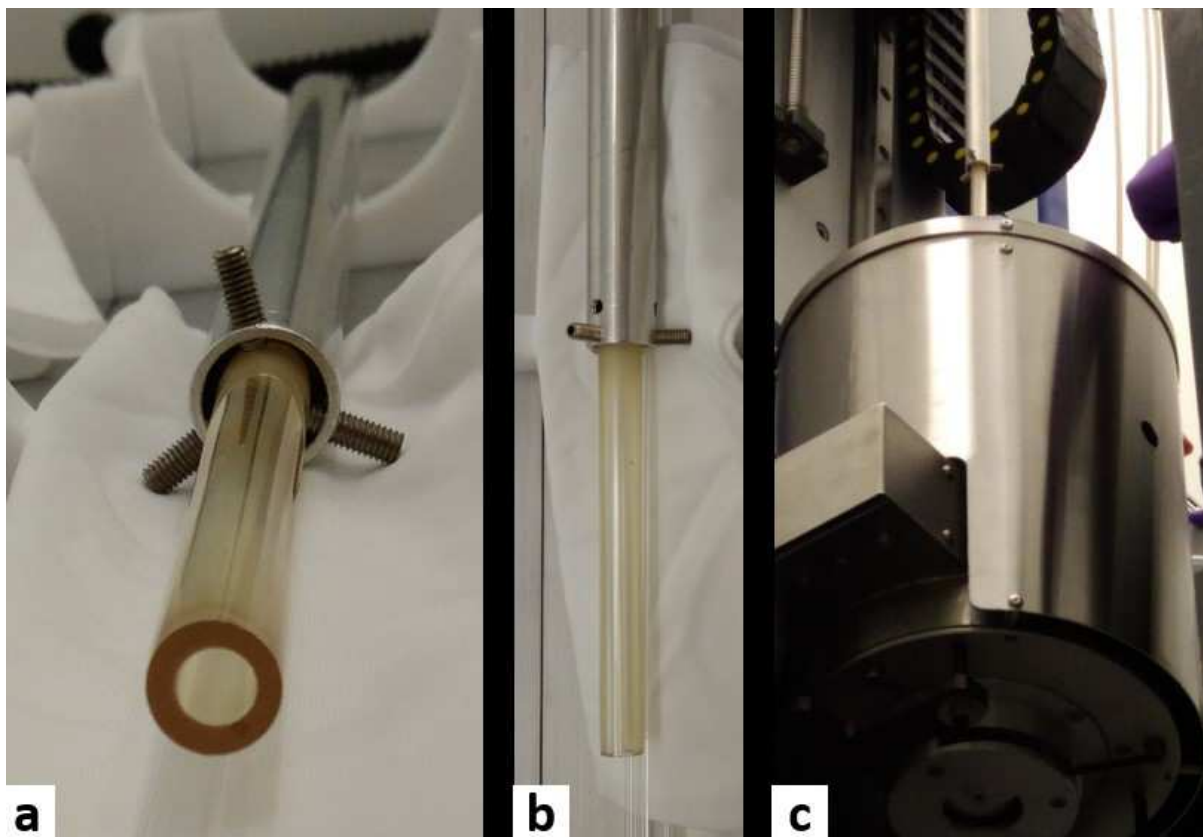


Figure 3.3. Photos showing one of the tubes obtained by rotational casting at Politecnico di Torino. The sample is positioned inside a tube of aluminum alloy 6061 and held with three screws (a, b), in order to be placed vertically in the drawing tower (c).

3.2 Stack and draw method for microstructured fibers

In the particular case of microstructured optical fibers (MOF), a second step besides the realization of the first preform is required. Indeed, MOFs have several holes, which are usually obtained with the *stacking technique*, consisting in piling up, by hand, capillaries and/or rods to create the correct geometry on a macroscopic level.

Other techniques such as molding, drilling and extrusion are applicable fundamentally to polymers, due to their great ductility that allows to design a wider number of configurations. In our case, however, the high brittleness of tellurite glass precludes the possibility to undergo other methods than *stack and draw*, which was then selected as the most recommended one.

To do that, generally two tube preforms are required: one destined to be drawn in order to get some capillaries, one that is employed as jacket during the stacking phase. The use of a recrystallization resistant glass is essential to obtain a good and stable quality of the final elements.

Different structures are achievable playing with parameters such as shape and diameter of holes, type of lattice and lattice pitch, leading to the chance to engineer the propagation properties of the optical fiber. Once the macroscopic preform with the predefined geometry is realized, it is drawn into the cane, an intermediate preform that shows the desired final structure but at the order of a few millimeters (Figure 3.4).

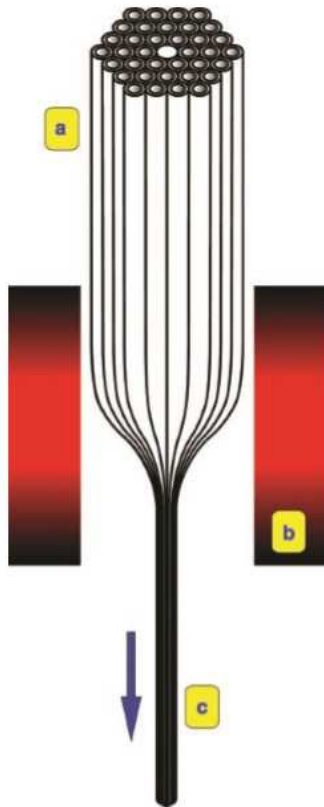


Figure 3.4. Illustration of the stack and draw procedure. The macroscopic preform with the desired structure (a) is placed in the drawing tower, fused together inside the furnace (b) and drawn down to intermediate preform (c) (figure retrieved from [24]).

Generally speaking, the stack and draw technique considers several consecutive steps, which may change a little bit depending on the specific system involved. The exact procedure carried out at The University of Central Florida for the realization of microstructured TZN fibers has been as follows:

1. One of the tellurite tubes received from Torino (Figure 3.3) was softened and drawn with the aim of fabricating capillaries of the desired dimensions for the decided geometry. The process was run with a preform feeding speed of 3 mm/min and a draw

speed of 0.347 m/min. The furnace temperature varied between 340 °C and 385 °C during the trial, in an attempt to find the most appropriate conditions.

Unfortunately, the material behaved in a manner not expected, continuously changing its viscosity over time. Consequently, it has not been possible to get capillaries with the diameter wanted, since the transverse sizes were repeatedly differing. The outer diameter of the samples ranged from around 0.42 mm to 1.1 mm, while the inner diameter from 0.01 mm to 0.43 mm (Figure 3.5).

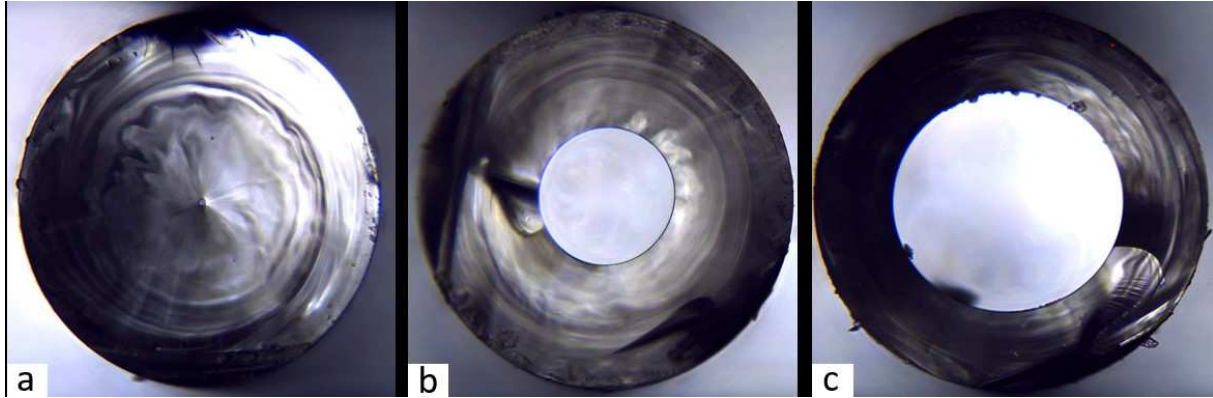


Figure 3.5. OM cross sections of three capillaries obtained after the tube's drawing. Size of outer diameter: a) 0.53 mm, b) 0.57 mm, c) 0.69 mm. Size of inner diameter: a) 0.01 mm, b) 0.21 mm, c) 0.41 mm.

This unpleasant result is due to the fact that tellurite, if compared to silica, presents a far smaller temperature range suitable for pulling, since the viscosity changes much more brusquely with temperature and makes the process very complicated.

Luckily, after an accurate examination, three pieces with quite constant dimensions were found. Specifically, their outer diameter (OD) and inner diameter (ID), from one side to the other, as well as their corresponding length, are summarized in Table 3.1.

Table 3.1. Relevant sizes of the three most dimensionally stable capillaries obtained after the drawing.

	<i>OD (Top)</i>	<i>ID (Top)</i>	<i>OD (Bottom)</i>	<i>ID (Bottom)</i>	<i>Length</i>
Sample 1	0.745 mm	0.270 mm	0.710 mm	0.330 mm	~ 96 cm
Sample 2	0.720 mm	0.260 mm	0.730 mm	0.190 mm	~ 101 cm
Sample 3	0.660 mm	0.430 mm	0.690 mm	0.410 mm	~ 85 cm

Therefore, a new geometry was conceived with the idea of using the material from samples of Table 3.1 for the inner part of the fiber structure. In fact, the aim was to employ, for the region around the core, the best pieces available in terms of material quality and dimensional stability, in order to enhance as much as possible light propagation along the fiber. On the other hand, the remaining space was filled up making use of the other pieces at disposal, which had greater dimensional variability. Since the latter ones were mainly placed in the outer part of the arrangement, they would interfere less with guiding properties.

- The capillaries obtained after drawing were cut into shorter parts according to the design selected and the length of the second tube (110 mm), which was employed as jacket.

The structure was designed taking into account that the amount of material available for the stacking was very little. Furthermore, the intent was also to take full advantage of the preform trying to get at least two different microstructured fibers from it. As a consequence, it was decided to totally fill up just the first half of the tube (Configuration A) and to create only one outer ring of capillaries in the second half (Configuration B). Figure 3.6 and Figure 3.7 help to understand the concept.

TUBE B: OD 10.8 mm, ID 6 mm

● 10 x OD 0.67 mm, ID 0.42 mm, length 5.5 cm

● 18 x OD 0.72 mm, ID 0.23 mm, length 5.5 cm

● 2 x OD 0.72 mm, ID 0.30 mm, length 11 cm

● 1 x OD 1,02 mm, length 5.5 cm

● 5 x OD 0.71 mm, ID 0.33 mm, length 5.5 cm

● 7 x OD 0.68 mm, ID 0.18 mm, length 5.5 cm

● 10 x OD 0.60 mm, ID 0.19 mm, length 5.5 cm

● 1 x OD 0.42 mm, ID 0.14 mm, length 5.5 cm

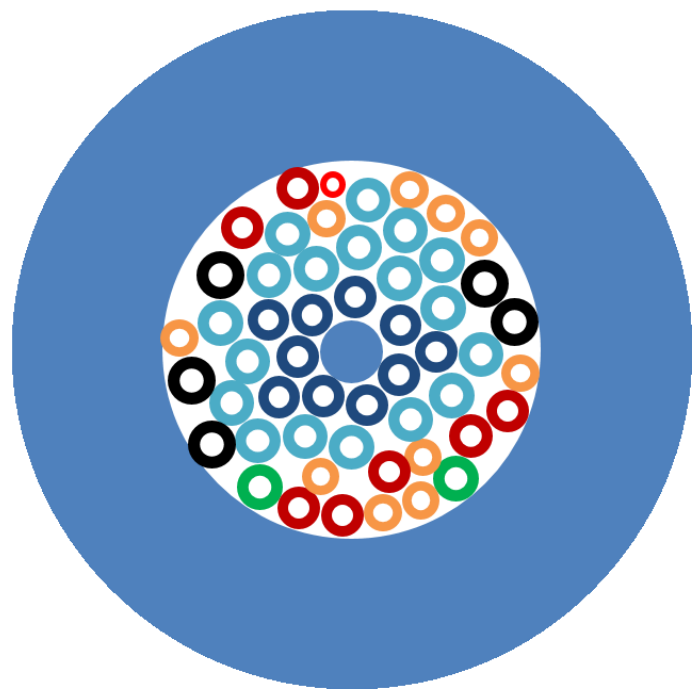


Figure 3.6. Simple schematic representation of the fiber optic design chosen for the first half of the preform (Configuration A). The configuration refers to a single core PCF structure. OD, ID and length of capillaries used to fill up the tube are also reported.

TUBE B: OD 10.8 mm, ID 6 mm

○ 6 x OD 0.72 mm, ID 0.30 mm, length 11 cm

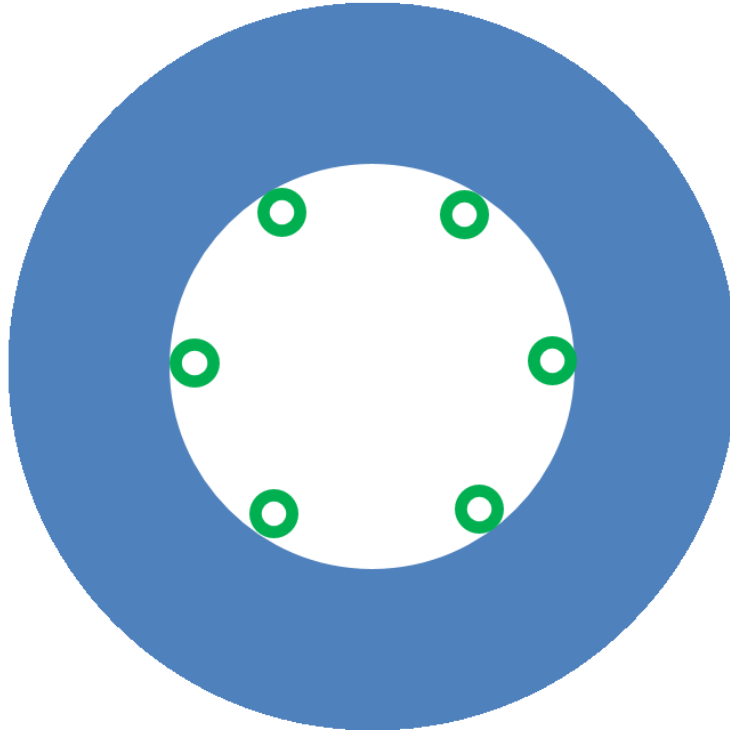


Figure 3.7. Simple schematic representation of the fiber optic design chosen for the second half of the preform (Configuration B). The configuration refers to an antiresonant hollow core structure. OD, ID and length of capillaries used to fill up the tube are also reported.

As can be seen, “Configuration A” is not accurate, since the employment of capillaries having so many different sizes makes it impossible to realize a symmetrical geometry. However, the scheme turned out to be a useful guideline during the stacking, especially to achieve a good structure in the central region. In fact, all the attention was focused on the obtaining of the first ring of 7 identical capillaries around the core, whereas the remaining space was piled with fewer restrictions.

Moreover, the decision to leave almost empty half of the tube was essential in order to acquire enough material. In this way, indeed, the number of pieces available doubled, because they were cut just 5.5 cm long. With regard to top-quality samples (Table 3.1), 18 capillaries were collected from “sample 2” and 10 from “sample 3”. The only pieces 11 cm long were obtained from “sample 3”; their role will be clarified later. Also other samples were used to get more pieces, which were prepared and divided by size. The inventory can be find in Table 3.2.

Table 3.2. Inventory of the pieces prepared for the stacking phase, with their relative sizes.

<i>Quantity</i>	<i>OD (μm)</i>	<i>ID (μm)</i>	<i>Length (cm)</i>
6	705 ± 15	300 ± 30	11
18	725 ± 5	225 ± 35	5.5
10	675 ± 15	420 ± 10	5.5
7	680 ± 30	175 ± 15	5.5
10	600 ± 20	185 ± 25	5.5
5	710 ± 10	335 ± 5	5.5
1	415	140	5.5

“Configuration A” was conceived with the intention of fabricating a single core PCF, whose microstructure consists of a solid core encircled by air-holes forming a periodic lattice. Since it is an index guiding fiber, it still transmits light due to the principle of TIR, just like traditional fibers. Its transmission properties depend on the size of holes and on the lattice pitch.

The realization of a dense core was not simple, since all the source material was in the form of capillaries (hollow objects). Firstly, it was attempted to taper one capillary using a GPX3400 Vytran Automated Glass Processor, whose working principle consist in applying heat on a short segment of the piece and, once the glass softens, stretch it in order to make it thinner. Thus, a reduction in diameter can be performed. Nonetheless, this strategy was shelved because it turned out to be too intense for a brittle glass like tellurite. In fact, albeit the softest parameters were used, the process still ended up with a break of the sample.

In the end, it was opted for assembling the core using the two pieces shown in Figure 3.8.

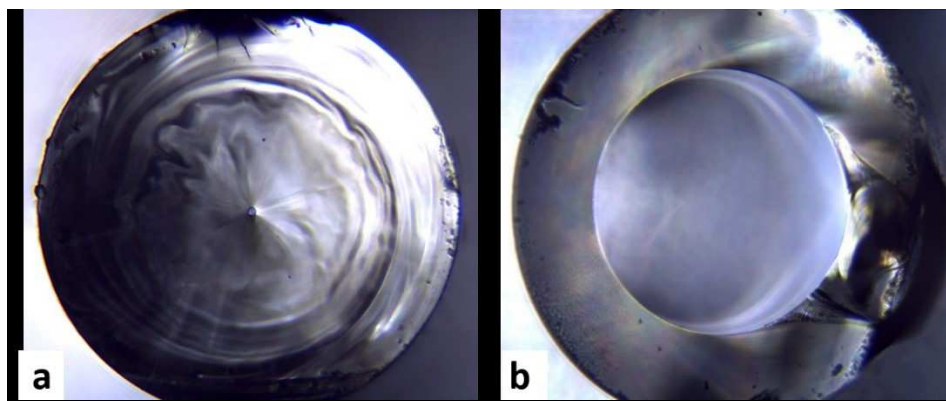


Figure 3.8. OM cross section of the two capillaries utilized to build the solid core. Size of outer diameter: a) 0.53 mm, b) 1.02 mm. Size of inner diameter: a) 0.01 mm, b) 0.59 mm.

As can be seen, among the capillaries available there was one almost collapsed (sample a). However, since its OD was too small with respect to the sought size, it was inserted inside a second capillary. Luckily, the OD of “sample a” matched perfectly the ID of “sample b”. Hence, a solid core of 1.02 mm diameter and 5.5 cm length could be prepared. The little amount of hollow space still present would disappear during the drawing into fiber.

“Configuration B” (Figure 3.7), instead, was designed with the purpose of fabricating an antiresonant hollow core fiber, which transmits light by photonic bandgap effect. It sticks out because here the core is an air hole, surrounded by a cladding structure of other air holes periodically arranged. This kind of structures follow the principle whereby guidance properties primarily depend only on the first layer enclosing the core. This single ring can be composed of any number of circles, frequently from 6 to 10. It is important to keep in mind that their dimension is regulated by the pressure applied during fiber drawing. Indeed, at the end of the fabrication their walls have become thinner and their air fraction has increased, as illustrated in Figure 3.9.

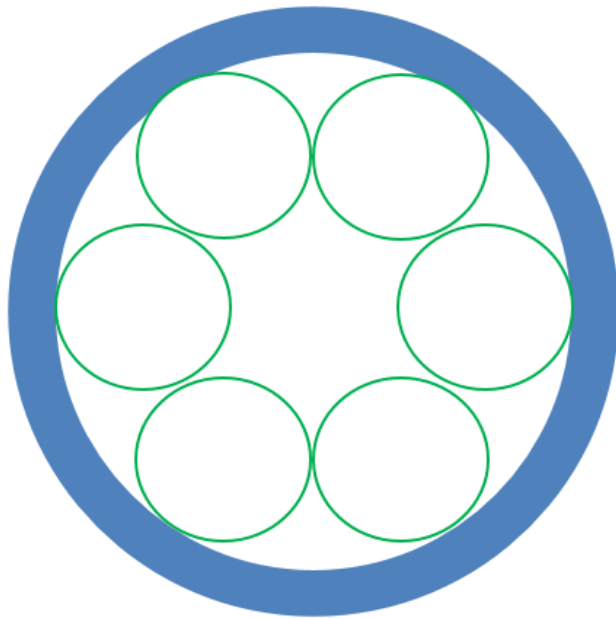


Figure 3.9. Typical structure of an antiresonant hollow core fiber, composed of 6 circles around the air core. It represents the type of microstructured expected from “Configuration B”.

3. According to the designed structure, a macroscopic mosaic was assembled by stacking the capillaries procured in step 2. This stage is crucial for the success of the entire procedure, since the manner the preform is realized determines the propagation properties of the final product.

Before proceeding with the stacking, a few more important adjustments were made. First of all, one end of every capillary was burnt and collapsed in order to close the hole from that side. To do that, a hydrogen flame was used. This operation is necessary to avoid unexpected movements of the pieces during fiber drawing, when vacuum is applied to adhere the six building blocks of the antiresonant part to the wall of the tube. Therefore, during preform preparation the collapsed sections were directed towards the upper side of the tube. Figure 3.10 facilitates the comprehension of this idea.

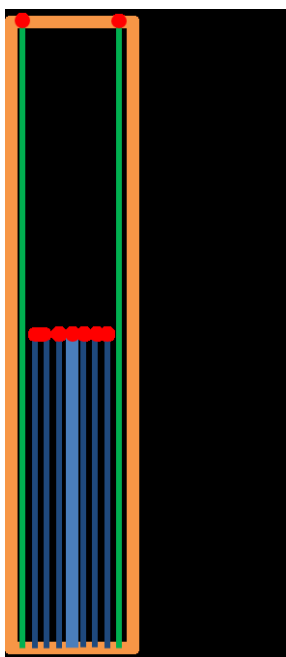


Figure 3.10. Schematic lateral view of the preform depicting how the capillaries are arranged inside the tube (in orange). Red points represent the collapsed side of the pieces.

Secondly, both tube and capillaries were cleaned up with acetone in preparation for the piling. Lastly, every not collapsed tip was painted with different colors according to size. This expedient helped a lot successive pieces identification inside the preform.

Done that, the main issue was to find a way to achieve both configurations. In fact, since the central region of “Configuration B” was empty, there was no manner for the longest capillaries to remain held against the wall autonomously. Consequently, the strategy adopted was to stack just two of them concurrently with shorter pieces, because if put in the underside of the tube they were able to sustain themselves. The remaining four were inserted afterwards, as will be discussed later in more detail.

Hence, the making of “Configuration A” was carried out. Since the material used was very heterogeneous, there was not a good control over disposition and it took several attempts to obtain an adequate outcome (Figure 3.11).

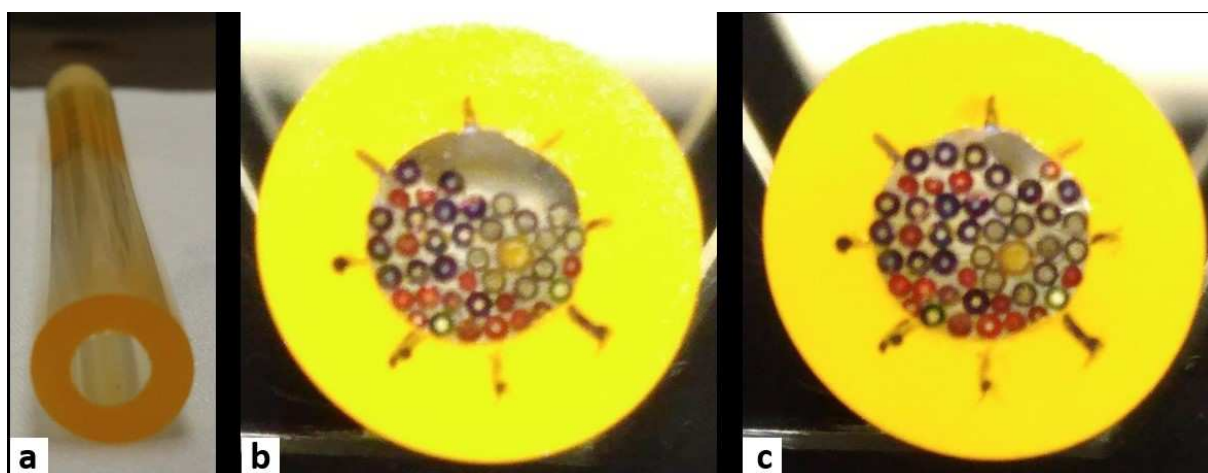


Figure 3.11. Different steps during the stacking phase. The tube (a), used as jacket, was gradually filled up with capillaries (b, c). The two green capillaries in the underside, which are twice the length of the others, continue up to the end of the tube.

Comparing Figure 3.11c with Figure 3.6, it is noticeable that the actual design differentiates from the original one. Particularly, the core, which is bigger than the capillaries and has a color similar to the tube, is quite off-center (Figure 3.12). Nevertheless, this is not a problem because light can propagate anyway. Indeed, in view of the difficulties to have a perfect geometry, it was decided to focus all effort on getting a satisfactory first ring around the core, regardless of its position. To do that, only capillaries from “sample 3” were used, since they were the most constant in terms of inner diameter. What models the optical behavior of the final fiber, in fact, is exactly the inner diameter of the pieces, whereas the outer diameter is important to consider just in order to know the space occupied by each one inside the arrangement.

In first approximation, then, light is confined just in the core region and the influence of more distant air-holes over propagation is irrelevant. Thus, it can be concluded that the role of the capillaries located out of the first ring is mainly to hold up the whole structure. That is why having the core precisely in the center is not essential for a first trial. It becomes relevant only if operations such as splicing are planned on the fiber.



Figure 3.12. Front view of “Configuration A” that highlights the core and the first ring of 7 capillaries around it.

Once “Configuration A” was completed, it began the placement of the antiresonant part from the other side of the tube. Since two capillaries had already been inserted, only four of them were still required. The approach taken was to tape them to a silica tube using polytetrafluoroethylene (PTFE) seal tape and, afterwards, introduce the whole thing inside the preform (Figure 3.13). Since the ID of the TZN tube was 6 mm, the silica tube was specifically fabricated with a OD of 4.5 mm in order to give the exact space for the capillaries to fit in.

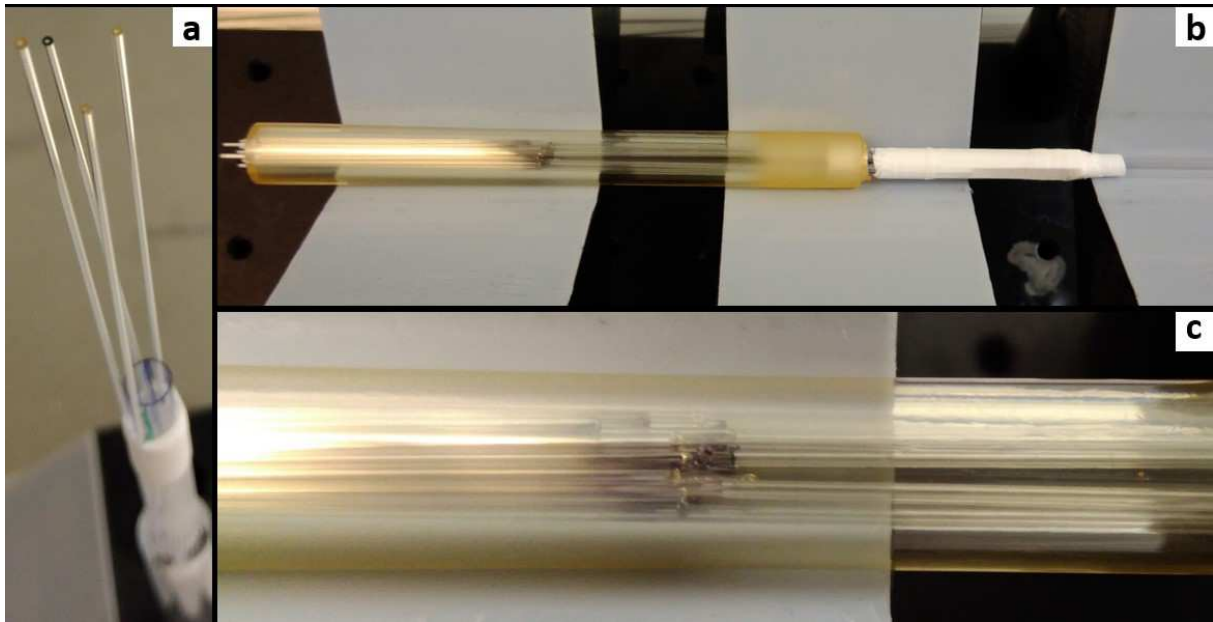


Figure 3.13. Different steps during the stacking of “Configuration B”. The four remaining capillaries were taped to a silica tube (a) and then introduced inside the TZN preform (b) until they touched the pieces belonging to “Configuration A” (c).

In addition, the calculation was made so that the silica tube would go into just the first centimeter of the preform, which is roughly the length that will be lost in any case during fiber drawing. The aforementioned length resulted to be enough to sustain the four capillaries and keep them quite in touch with the wall. A better contact is then achieved once vacuum is applied inside the drawing tower. This last aspect is crucial to obtain a good structure for the antiresonant fiber. It is also important to point out that, in this case, the application of PTFE seal tape did not make it necessary to burn and collapse one end of the pieces.

A tube of aluminum alloy 6061 was then specifically fabricated to hold the preform vertically during the following drawing phase and allow the application of vacuum. It was tightened around the last 1 cm of the TZN preform.

The final step of the stacking was to melt the very beginning of the preform for the purpose of sticking together capillaries and jacket and, so, avoid their fall during vertical positioning. It was first tried to use the same hydrogen flame previously utilized but, unfortunately, the heat supplied was too high for the TZN tube and led to evident damage. In particular, a segment of material literally broke down (Figure 3.14a). Therefore, a different strategy had to be taken to prevent further complications. A Thermo Scientific Lindberg/Blue M Tube Furnace was employed to carefully control temperature over preform’s front end, which was inserted through the opening of the oven (Figure 3.14b, Figure 3.14c). The segment was heated above its T_g and periodically rotated to attain a homogeneous softening. The final result was satisfactory (Figure 3.14d).

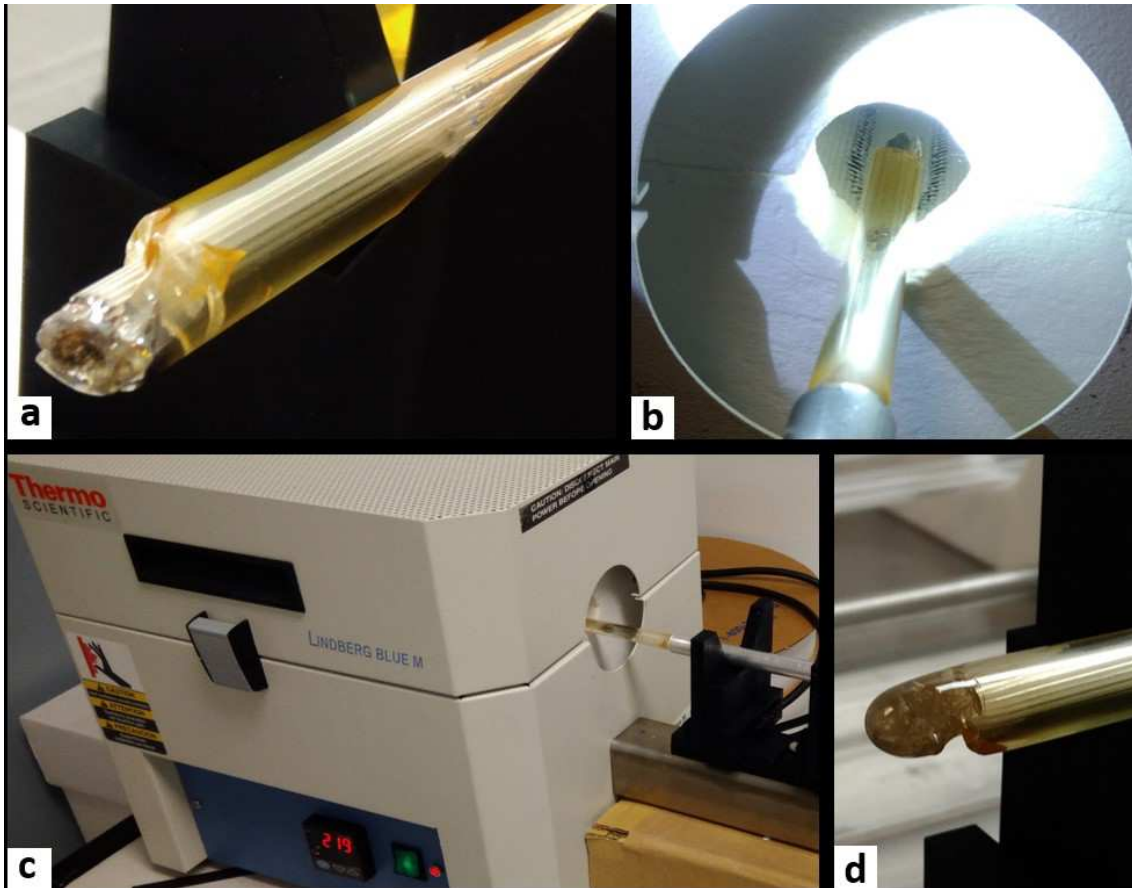


Figure 3.14. The damaged extremity of the preform (a) was put inside a tube furnace (b) and heated above its T_g (c). At the end of the process the piece had softened as expected (d).

4. Once the stacking phase was concluded, the preform was ready to be firstly drawn into a cane (intermediate preform) and then into the final fiber.

In order to be able to apply vacuum, a tube adapter for pressure fitting was connected to the tube of aluminum alloy. Then, the whole thing was placed vertically at the top of the drawing tower (Figure 3.15).

The procedure was run with a preform feeding speed of 2 mm/min and a draw speed of 17.6 m/min. The furnace temperature was slowly increased up to 340 °C and vacuum was also applied to preserve the internal structure.

Standardly, fiber optics have an outer diameter of 125 μm , but several other sizes might be manufactured in order to tailor their properties. In this specific case, it was selected a diameter of 115 μm that led to a core diameter of 10 μm , which is a suitable dimension for single-mode propagation.

Furthermore, as in this case both core and cladding are made of the same glass (equal glass transition temperature and coefficient of thermal expansion), no concerns are needed regarding the possible formation of significant internal tensions during solidification.

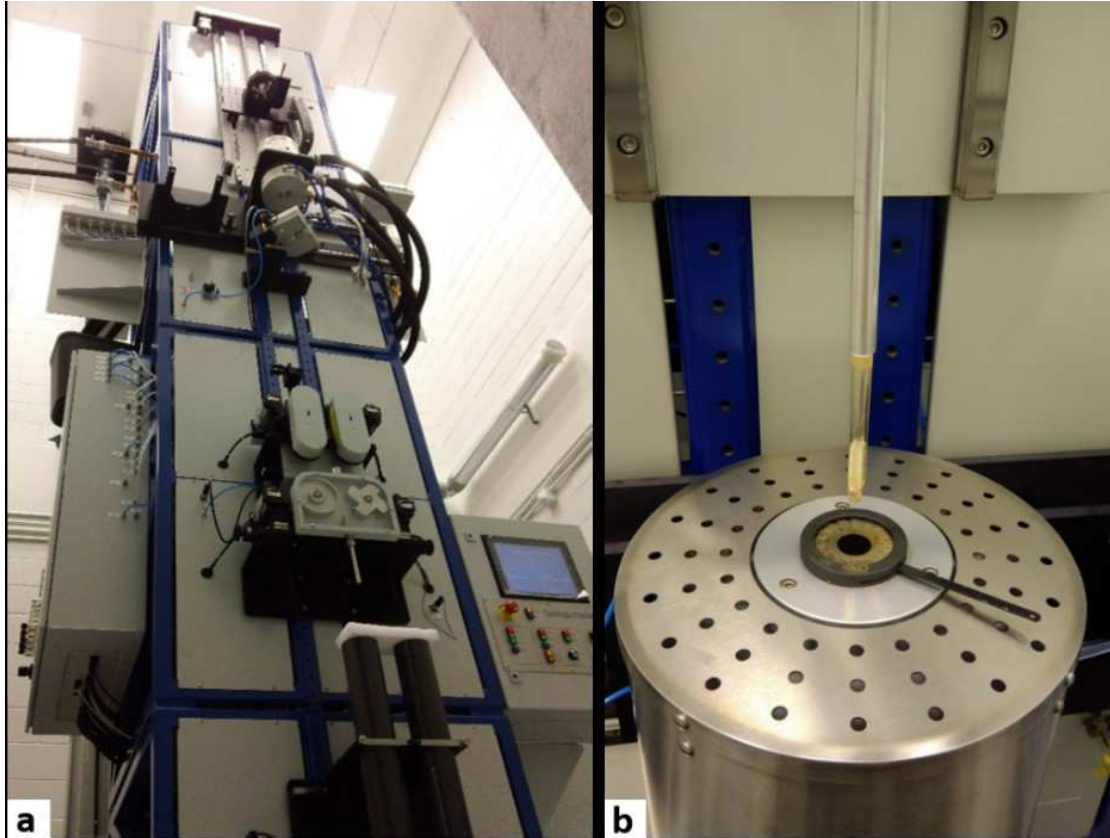


Figure 3.15. Pictures showing the drawing tower utilized (a) and the preform placed vertically and ready to be lowered inside the furnace (b).

However, the trial failed due to an unexpected fall of the preform from the top to the ground. This unfortunate event occurred just when the pulling had started and provoked the formation of cracks on the sample (Figure 3.16). Thus, no optical fiber was obtained.

The possible causes of the incident will be analyzed and discussed in Section 3.3.



Figure 3.16. Picture of the preform that turned out to be visibly damaged after falling from the drawing tower.

3.3 Results and discussion

Tellurite glass is a brittle material and must be handled with care. This aspect increases the difficulties faced during the process of fiber fabrication, especially if the amount available is scarce. Moreover, since its physical properties differ widely from the ones of silica, it took a lot of time to find alternative solutions that could be used. In particular, the main issues encountered have been:

- achieve a good control over glass viscosity variations with temperature and, thus, over the entire drawing procedure. Indeed, here the temperature range is much narrower compared to silica and requires a bit of practice to identify the right parameters. This inexperience led to the obtaining of dimensionally irregular capillaries, with sizes quite different from the ones originally desired;
- design the configuration and carry out the stacking utilizing capillaries having variable outer and inner diameters. This nonideal situation is the reason it was not doable to make a symmetrical structure and position the core in the center;
- the impossibility of stabilizing preform structure by using a flame once the stacking was completed. A tube furnace was employed instead, making the process more difficult and time-consuming. On top of that, in an attempt to accomplish the task, the first part of the preform was ruined;
- the need to manufacture a tailored aluminum alloy tube for vacuum application, different from the one used during capillaries fabrication (Figure 3.3). The end of the preform that eventually cracked and caused the fall of the entire piece was exactly located inside this new component.

Therefore, despite the extreme caution used, an unexpected fracture at the top of the preform during fiber fabrication precluded any possibility of making the desired fiber.

As mentioned, the breakage involved the part of the preform situated inside the aluminum alloy tube (Figure 3.17). Hence, the cause of failure should be investigated in that portion.

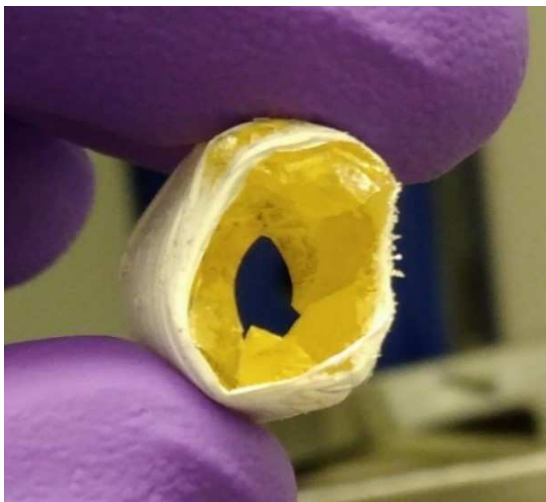


Figure 3.17. Picture that shows preform extremity formerly housed inside the aluminum alloy tube. Its breakdown caused the fall of the entire preform.

First of all, it is reasonable to have a look at the coefficient of thermal expansion of the two materials involved. With regard to the glass, it has a CTE of $18.8 \times 10^{-6} \text{ K}^{-1}$ over a temperature range between ambient and $250 \text{ }^\circ\text{C}$, as will be discussed in detail in Subsection 4.1.2. The value for aluminum alloy 6061, instead, is easily accessible and equal to $23.6 \times 10^{-6} \text{ K}^{-1}$ (20-100 $^\circ\text{C}$) [25]. The difference between them results in $4.8 \times 10^{-6} \text{ K}^{-1}$, if a consistent temperature window

is considered. It is a value definitely non-negligible, although it should not pose a significant risk considering the relatively low temperatures reached. Additionally, it is important to note that the main issues usually take place during cooling, when the different shrinkage behavior means that internal tensions originate at the interface. Especially, compressive stresses arise on the material with lower CTE and tensile stresses appear on the other. Once cooling is completed, these residual stresses remain inside the material if no method for relief is adopted. Nonetheless, since in this case did not occur a temperature reduction, the reason of failure must be sought elsewhere.

The hypothesis that the inner diameter of the metallic tube did not match the outer diameter of the TZN tube is also unlikely, since a clear separation took place between the segment of glass inside the aluminum component and the rest of the preform. This demonstrates that the TZN extremity was sufficiently held tight. Otherwise, if the aluminum alloy tube had been too large, there would have been backlash between the parts, leading to a relative motion and, thus, to the fall of the whole preform.

On the other hand, it seems the several operations executed previous to fiber drawing were the actual cause of the incident, since some of them led to slight damage on the end of the preform. In fact, prior to employing the aluminum alloy tube, another strategy was attempted to permit vacuum implementation. During that action, which consisted in joining the TZN tube to a silica tube by means of two brass fittings (Figure 3.18), a small crack formed, revealing that it was not the perfect solution. Hence, it was decided to replace the silica tube with the aluminum alloy one, but by then the damage was there.

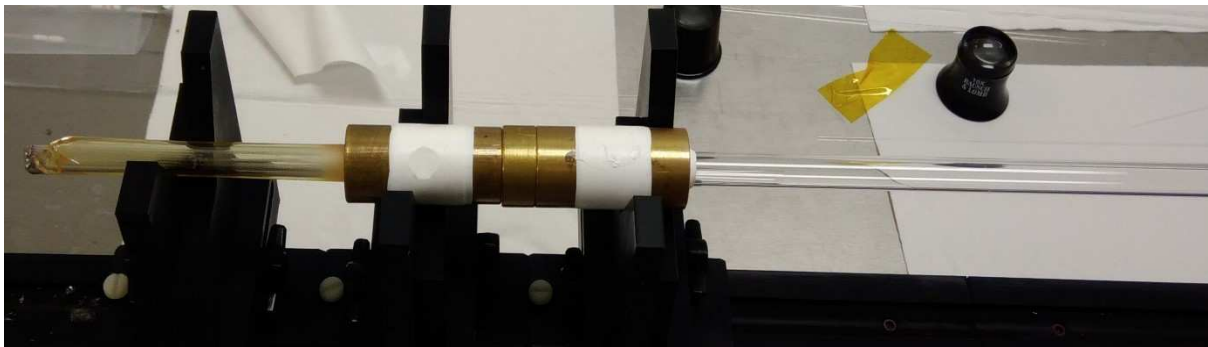


Figure 3.18. Image showing the joining between the TZN tube (on the left) and the silica tube (on the right) realized by means of two brass fittings (in the center).

The defect didn't seem alarming in that moment but, in hindsight, it is likely that its propagation was the cause of the fracture. Indeed, the cave-in occurred when a TZN rod was introduced inside the furnace from the bottom with the intention of detaching a part of the preform stuck to the wall. Presumably those stresses exerted on the preform, aided by the heat that was inside the chamber, led to crack growth and, consequently, to the final failure.

In view of all this, it might be concluded that the ultimate strategies implemented appear to be adequate for the processing of this TZN glass, since the unpleasant result of this work is just due to inexperience. In fact, it was the necessity of investigating different approaches that led to critical damage.

Therefore, now that the most suitable conditions have been identified, everything suggests that the next attempt to fabricate the fiber will have a much better chance of success, taking always into account that extreme caution is required.

4 Characterization

Characterization and analysis were performed on TZN glass. Several features were investigated in order to better understand the properties of the material and gain greater insight into its behavior when applied in desired applications.

All measurements and tests were carried out at University of Central Florida.

4.1 *Thermo-mechanical and mechanical properties*

Significant engineering issues are strictly related to how some materials properties change with temperature or external stresses. In the specific case of fiber optics, indeed, the possible conditions of operation often require an attentive analysis and understanding of such circumstances. Therefore, it was indispensable for our tellurite glass to undergo some mechanical and thermo-mechanical measurements, including differential scanning calorimetry (DSC), dilatometry, viscosity and hardness. However, since tubes fabrication does not produce residual material, the only pieces of tellurite glass usable for characterization were the remains from the drawing of such tubes. Thus, considering that no facilities to process the glass were available and both viscosity and dilatometry measurements require specimens of specific size and shape, it was not possible to realize such analyses. For the latter, a research on other publications was done in order to get some approximate values that could give an idea about viscosity (η) and coefficient of thermal expansion (CTE).

4.1.1 DSC – Differential Scanning Calorimetry

As already discussed in Chapter 2, an amorphous material like tellurite glass is in metastable state of equilibrium. According to thermodynamics, this means that its structure can change if one or more thermodynamic magnitudes vary, affecting its properties as a result. In this regard, *differential scanning calorimetry* can be an excellent tool to investigate how the material reacts and potentially undertakes a phase transformation when temperature is increased.

The instrumentation consists basically of two identical pans arranged in a chamber, where the temperature can be raised or decreased by two independent heaters and monitored with sensors. The sample to be examined is placed in one pan, whereas the empty one works as a reference. If for both pans the same heat rate ($\Delta T/\Delta t$) is set up, a different heat flow ($\Delta Q/\Delta t$) will emerge, since the presence of the material leads to a higher heat capacity. Thus, a heat flow versus temperature graph can be plotted.

When a specific temperature is reached, a first order phase transition occurs and a latent heat (released or absorbed) is associated with it. Second order transformations, instead, do not possess a latent heat but cause a change of the heat flow, too. Therefore, all these important thermal phenomena can be detected. Melting and boiling points, crystallization events, glass transition temperature and chemical reactions are just some of the many that can be observed with DSC equipment.

The analysis was carried out on a tellurite glass fragment acquired from tube 1 (Figure 3.3) after the drawing, using a TA instruments DSC Q10 (Figure 4.1).



Figure 4.1. TA instruments DSC Q10 utilized for the differential scanning calorimetry measurement.

The sample, with a weight of 21.9 mg, was put between a crucible and a lid, both made of aluminum, and sealed by means of a crucible sealing press. After being placed inside the machine, it was first brought to 200 °C and equilibrated; then, it was heated up to 500 °C at a heating rate of 10 °C/min. As purge gas, an argon flow of 50 ml/min was blown at atmospheric pressure in order to maintain an inert environment.

Since the amount of material available was scarce, only one measurement was performed. Nonetheless, the temperatures of interest were found to be far different from each other, so that, examining the data with respect to fiber drawing, even an error of ± 5 °C (unlikely) would not be a problem. The results are shown in Figure 4.2., where the heat flow is considered exothermic.

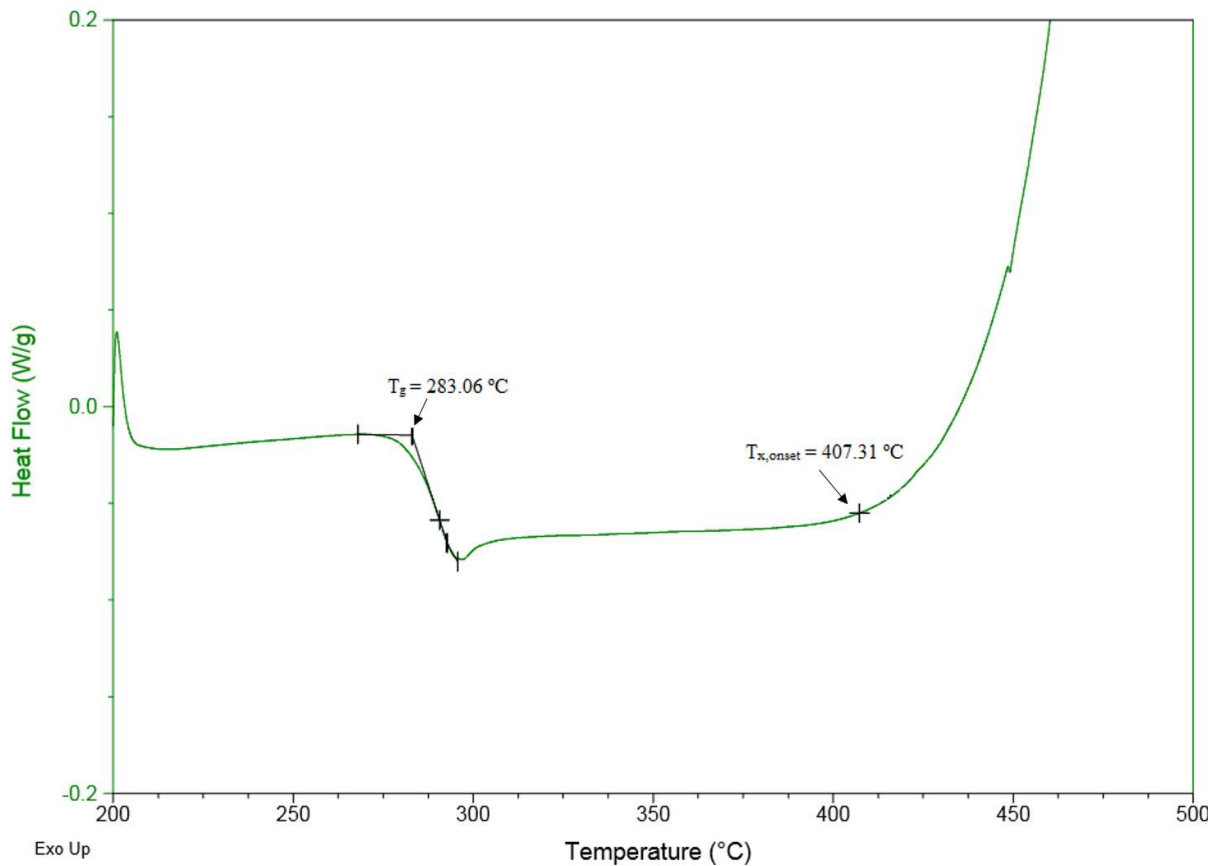


Figure 4.2. DSC spectrum of TZN glass with corresponding glass transition temperature T_g and crystallization onset temperature $T_{x,onset}$ indicated. Exothermic reactions are shown with a positive peak.

Within the temperature range analyzed (200-500 °C), two main events occur on the specimen: glass transition and the beginning of crystallization. A broader graph containing the whole shape of the curve is presented in Appendix 6.2.

Due to the relatively low melting point of the crucible of aluminum (660 °C) that restricted the maximum temperature reachable inside the chamber, it was not possible to identify the melting temperature of the glass which, in any case, would have been superfluous for this study.

According to the plot, the material starts to soften at a T_g value of 283 °C, whereas the crystallization begins at a $T_{x,onset}$ of 407 °C, temperature at which atoms start to arrange into a highly organized structure. Since in this case the formation of a crystal is undesired, $T_{x,onset}$ represents a limit that must not be exceeded.

Commonly, in order to estimate the suitability of the glass for optical fiber fabrication, the thermal stability is considered. This is evaluated via:

$$\Delta T = T_{x,onset} - T_g, \quad (4.1)$$

where ΔT represents the glass capability of withstanding a thermal process without incur crystallization.

Consequently, the ΔT calculated for the material under examination results to be 124 °C.

In general, a quantity higher than 100 °C is considered adequate for the drawing process, which must be obviously conducted at a temperature inside that range in order to avoid any crystallization. Although values greater than 150 °C are more advisable, it could be said that this TZN glass has a good stability against devitrification.

4.1.2 Dilatometry

Whenever a material is subjected to a thermal load, it shows a mechanical response. The magnitude which quantifies that reaction is the coefficient of thermal expansion, or CTE. Specifically, it describes the dimensional variation taking place when a change in temperature occurs.

Though the most general expansion (or shrinkage) is volumetric, to a first approximation the coefficient can be considered linear. Thus, the linear thermal expansion of an object can be written as:

$$dL = \alpha L dT, \quad (4.2)$$

where dL and dT represent respectively the change in length (in mm) and temperature (in K), L is the length at room temperature (in mm) and α is the linear CTE (in K^{-1}), which can then be defined as follows:

$$\alpha = \frac{1}{L} \frac{dL}{dT} \quad (4.3)$$

It is important to specify that α is always expressed as an average value for a specific temperature span, since it is temperature dependent. Moreover, in (4.3) the effect of pressure is ignored.

A dilatometry measurement can be performed either with a *TMA instrument* or a *dilatometer*. In the first method the geometry of operation is vertical, whereas in the second one is horizontal. In both techniques the specimen is situated on a stage in proximity to a thermocouple; a pushrod is then placed in contact with the sample, applying a constant force. When the system provides a cooling or heating treatment, the material changes in dimension and causes the motion of the pushrod, which is monitored with a linear variable differential transformer (LVDT). Using the data collected, a temperature vs. dimension change graph is plotted, from which α can be calculated as the slope of the curve.

Although there is not a default size for the specimen, during its preparation it is always required to follow some guidelines for its shape and dimension, according to the equipment in use. Specifically, the instrumentation available at CREOL, a TA Instruments TMA 2940, needs slices with 2 to 10 mm of width and more than 5 mm of thickness. As a consequence, it was not possible to perform the analysis with the irregular samples available.

However, the measurement on a glass of the same composition has already been carried out by Manning S., Ebendorff-Heidepriem H. and Monro T., who report a α equal to $18.8 \times 10^{-6} K^{-1}$ over a temperature range between ambient and 250 °C [26]. Although the latter was exposed to a slightly different thermal treatment with respect to the glass of this study, the value can be accepted as accurate.

In particular, since in this work both core and cladding are made of the same material, there is no difference in the CTE and, thus, no thermal stresses should originate after the drawing. Nevertheless, an attentive analysis on this matter would be required at a later time if attempts to fabricate plurimaterial TZN glass fibers will be made.

4.1.3 Viscosity

Glass processing optimization requires a deep analysis of material's viscoelasticity, especially for those procedures which are temperature and time dependent, including fiber drawing. In fact, thermal stability and the relationship between viscosity and temperature underpin the engineering of glass photonic fibers. While thermal stability is well investigated performing a DSC measurement, as already discussed in Subsection 4.1.1, the viscoelastic behavior can be

examined with several different techniques, depending on the flow regime of interest. Regarding the ranges of viscosity suitable for fiber drawing, *parallel plate method* is the most widely used. It allows to study viscosity between 10^3 Pa·s and 10^6 Pa·s, a softening region where the glass is above its T_g and is characterized by a viscous state.

Exactly as in many other techniques, a specific specimen geometry is required. In this respect, a solid cylinder is employed and pressed in the vertical direction between two horizontal flat plates. Data concerning the compression rate is collected and then utilized to determine viscosity by means of the following equation [27]:

$$\eta = 2\pi \frac{Mgh^5}{30V(dh/dt)(2\pi h^5 + V)(1 + \alpha T)}, \quad (4.4)$$

where η is the viscosity (in Pa·s), M is the applied load (in g), g is the gravitational acceleration (980 cm/s^2), h stands for the height of the sample (in cm) at time t (in s), V is the sample volume (in cm^3), dh/dt is the compression rate (in cm/s), α is the linear coefficient of thermal expansion of the material (in K^{-1}) and T is the operating temperature (in K).

Nonetheless, here too comes the same issue encountered for the dilatometry measurement, namely the impossibility to get a sample of size and shape required for the analysis. Again, a look at other publications was taken, but this time without finding studies on the same material. Up to now, indeed, viscosity of tellurite glasses has been investigated just for a few compositions.

However, in [28] Animesh Jha reports viscosity at different temperatures for an 80% TeO_2 , 10% ZnO , 10% Na_2O glass, which has a very similar composition to the one of this work. In fact, the DSC spectrum found in [29] assigns to it a T_g of $285 \text{ }^\circ\text{C}$, a value almost equal to the one showed in Subsection 4.1.1. Although its crystallization onset is slightly higher, at around $450 \text{ }^\circ\text{C}$, it can be deduced that the viscosity behavior of the two glasses is comparable.

The data given in [28] is the following:

- $\log\eta=12$ at $267 \text{ }^\circ\text{C}$;
- $\log\eta=10$ at $295 \text{ }^\circ\text{C}$;
- $\log\eta=6$ at $329 \text{ }^\circ\text{C}$;
- $\log\eta=3$ at $385 \text{ }^\circ\text{C}$.

As already said, the attention is focused on the range between $\log\eta=6$ and $\log\eta=3$. Especially, the proper temperature for fiber drawing of tellurite-based glasses is usually assumed to be the one corresponding to around $\log\eta=4$, where glass softening is sufficient for it to be successfully pulled to a diameter much smaller. However, the few values at disposal are not enough to make a curve, whose trend is always non-linear, as can be inferred from the observation of other viscosity curves of TZN glasses [19, 28].

Overall, some conclusions can still be drawn regarding the right temperature for fiber fabrication. For instance, it is safe to say that a furnace at $385 \text{ }^\circ\text{C}$ would be a too hot environment, whereas $329 \text{ }^\circ\text{C}$ represents a condition colder than the one required. Moreover, these last considerations match perfectly the permitted temperature span identified in Subsection 4.1.1, eliminating the risk of a potential crystallization event during the process and, thus, confirming once again the good thermal stability of the glass.

Taking all these facts into account and based on the experimental experience gained during the fiber drawings carried out, it can be said that the ideal working temperature is located between $340 \text{ }^\circ\text{C}$ and $360 \text{ }^\circ\text{C}$.

4.1.4 Hardness

Material hardness is defined as a measure of the resistance of its surface to indentation (technological concept), abrasion (mineralogical concept) and plastic deformation (physical concept). Although several testing methods are available to define it, *indentation hardness* is certainly the most used and recognized. It consists in creating an indentation on the surface of the material by applying a static compressive load for a certain time. When the indenter penetrates the specimen, it provokes a localized elastic deformation, followed by a plastic one that leaves an imprint. Then, hardness is determined by evaluating either the size of such imprint or the penetration depth of the indenter, according to the method used.

In this case, *Vickers microhardness* (HV) technique was used in order to have minimum damage on the sample (nondestructive test). HV is calculated dividing the applied load by the area of the mark, obtained with a diamond indenter in the form of a square-based pyramid and having an included angle of 136° . This particular shape gives to the imprint the geometry illustrated in Figure 4.3.

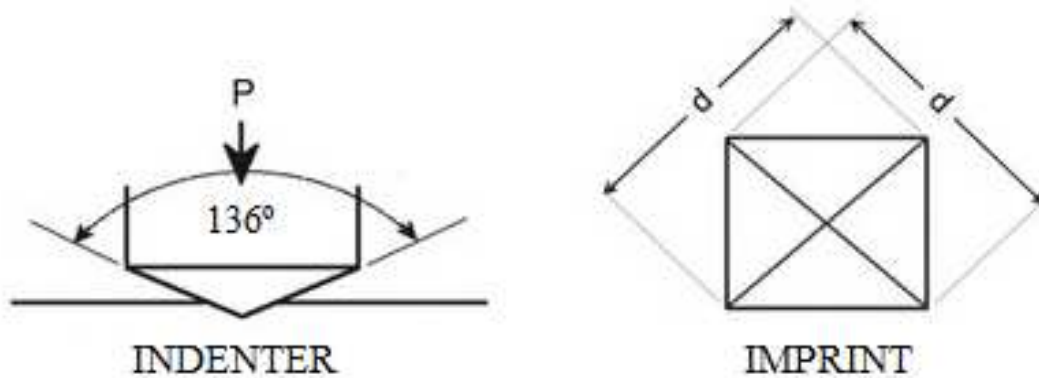


Figure 4.3. Schematic of a Vickers diamond indenter (left) and its resulting imprint on the tested surface (right).

Thus, it can be used the following equation:

$$HV = \frac{F}{A} = \frac{F}{d^2 / 2 \sin(136^\circ/2)} = 1.8544 \frac{F}{d^2}, \quad (4.5)$$

where F is the force on the diamond indenter (in kgf) and d is the diagonal length of the imprint (in mm). Therefore, HV is expressed in kgf/mm^2 .

If we want to have the same result but using SI units, the force must be converted from kilogram-force to newton:

$$HV = 1.8544 \frac{F/g}{d^2} = 1.854 \frac{F/9.807}{d^2} = 0.1891 \frac{F}{d^2}, \quad (4.6)$$

where this time F is in N, d in mm and HV in kgf/mm^2 .

Specifically, microhardness is the best option when dealing with brittle materials like tellurite glass. Since it refers to a test that employs a load of less than 1 kg, the damage created is very little and surface. On the other hand, it requires an accurate sample preparation in order to get a polished layer as regular as possible. This is necessary to have perpendicularity between indenter and surface and properly distinguish imprint size with the eyepiece.

The specimen used for the measurement was retrieved from the drawing of first tube (Figure 3.3). It was cut into proper size and then polished on both sides (Figure 4.4).

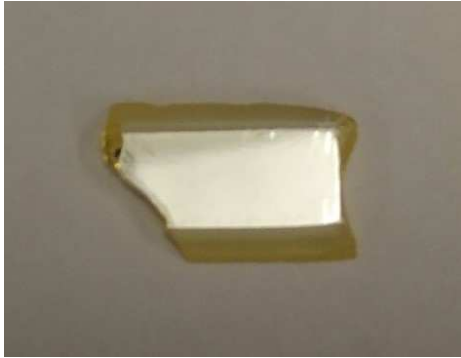


Figure 4.4. Image of the tellurite glass sample used for Vickers microhardness test. It was polished on both sides.

The equipment utilized was a Shimadzu DUH-211S (Figure 4.5) and the force, applied for 15 s, was equal to 100 mN.

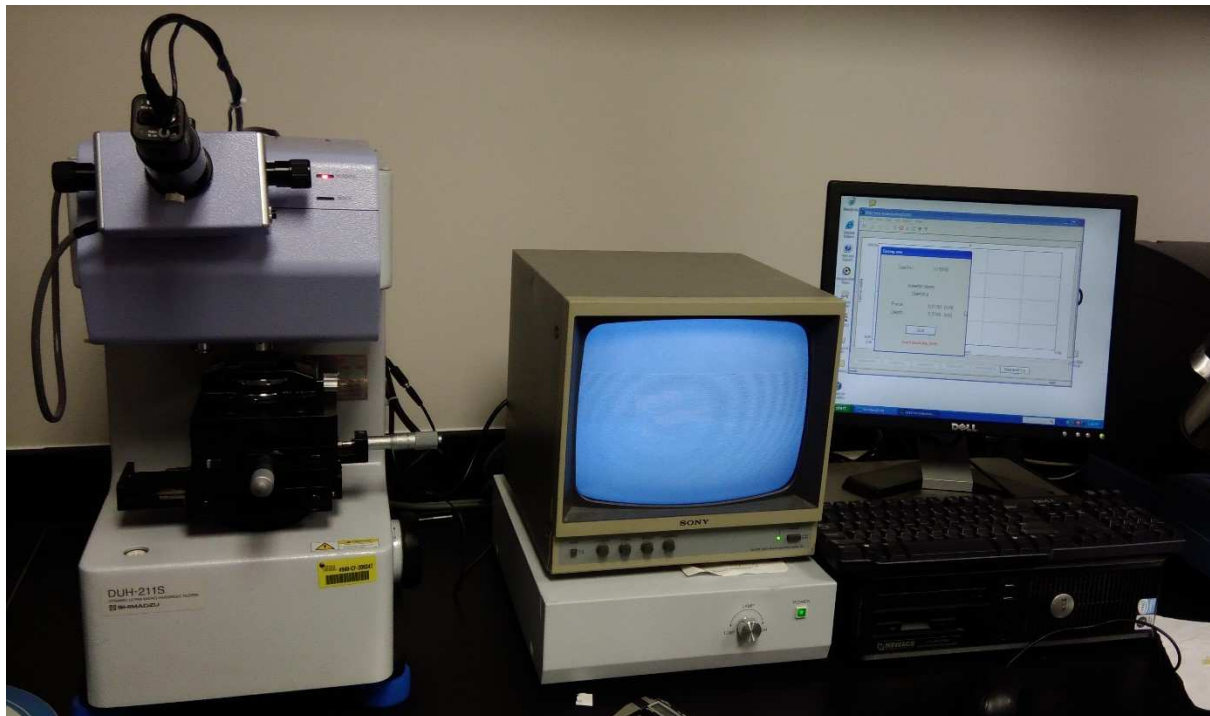


Figure 4.5. Shimadzu DUH-211S utilized for the Vickers microhardness measurement.

The test, performed at room temperature, was repeated 10 times on different zones of the sample sufficiently distant from each other, so that no alteration could result due to previous indentations. This strategy allowed to obtain an average value and minimize the error. Diagonals length was measured by means of a microscope. The result of the experiment is shown in Tab 4.1, where HV is calculated using (4.6).

Tab 4.1. Outcome of Vickers microhardness test on TZN glass sample. Applied load F , diagonal length d (average of the two) and resulting HV are reported for each indentation, along with mean value and standard deviation.

<i>Sequence</i>	<i>F [mN]</i>	<i>d [μm]</i>	<i>HV</i>
1	100.44	7.727	318.104
2	100.42	7.759	315.456
3	100.44	7.598	329.012
4	100.40	7.856	307.620
5	100.28	7.571	330.830
6	100.42	7.593	329.366
7	100.30	7.703	319.681
8	100.28	7.498	337.294
9	100.30	7.764	314.679
10	100.32	7.598	328.606
Mean value	100.36	7.667	323.065
Standard deviation	0.069	0.111	9.258

In addition to being a nondestructive measurement, the other main advantage of this hardness test is to be very simple to carry out. Moreover, since it evaluates a property of resistance of the material, the result can be related to other mechanical properties such as the tensile strength. Nevertheless, even though some empirical relationships between these two magnitudes have already been formulated, they are reliable just regarding a restricted number of materials (especially steels and cast iron). In any case, hardness test can be used to determine resistance to plastic deformation, as well as giving information about abrasion resistance. This last property is of particular interest for those fiber optics applications that involve harsh environmental conditions.

With regard to TZN glass, the value of 323 HV obtained is pretty low compared to silica, which shows at least 750 HV depending on several factors such as exact chemical composition and heat treatment undergone [30, 31].

Such small value reflects the behavior of the material during the experimental stage, where it has proved to be extremely brittle towards any type of external mechanical stress.

4.2 Refractive index measurement

For materials meant for optical applications, the refractive index (n) is an essential value to know, since it plays a major role in the final optical behavior. Among the techniques available to measure it, the *prism coupling method* was used. Its operating principle is based on the experimental setup reported in Figure 4.6.

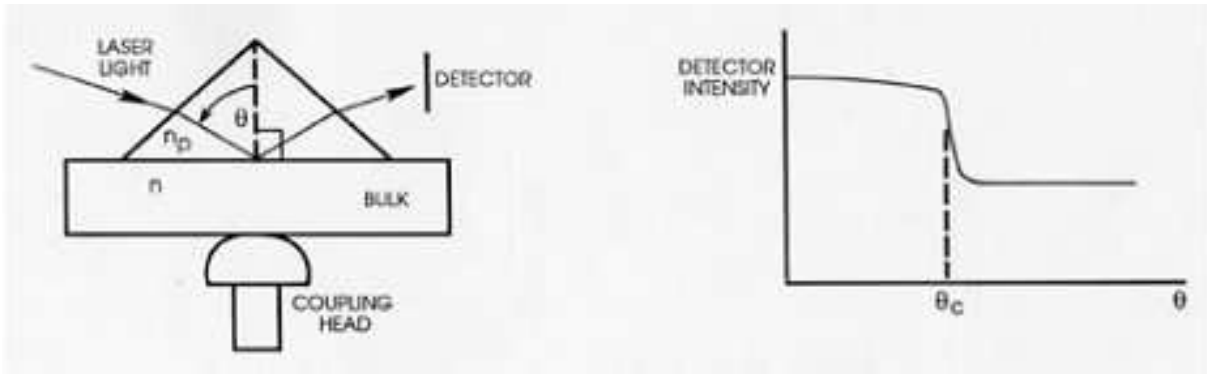


Figure 4.6. Schematic of experimental arrangement (left) and Angle versus Intensity graph (right).

The bulk material of unknown refractive index, in the form of a substrate, is pressed in optical contact with a prism by means of a coupling head. The prism material is chosen to have higher n than the substrate.

Laser light of defined wavelength is launched into the prism and is then reflected at prism base due to total internal reflection. A photodetector placed on the opposite side collects the intensity of the refracted light. The angle of reflection θ can be smaller or greater than the critical angle θ_c , depending on the incident beam incline. By means of a rotation stage, the angle of incidence is varied until the laser beam is coupled into the bulk material. This phenomenon is revealed in the Angle vs. Intensity curve by a sharp drop of intensity at θ_c , as illustrated in Figure 4.6 above. The coupling condition depends on θ_c for the sample/prism interface, n of the prism and n of the substrate. Since the latter is the only unknown quantity, it can be calculated. The value obtained depends on the laser wavelength used [32].

The instrumentation utilized was a Metricon Model 2010/M Prism Coupler, equipped with a high refractive index GaP prism and a $0.98 \mu\text{m}$ laser source (Figure 4.7). It provides a resolution of ± 0.0005 and requires a specimen with flat and parallel surfaces and with an area of at least 5 mm^2 .

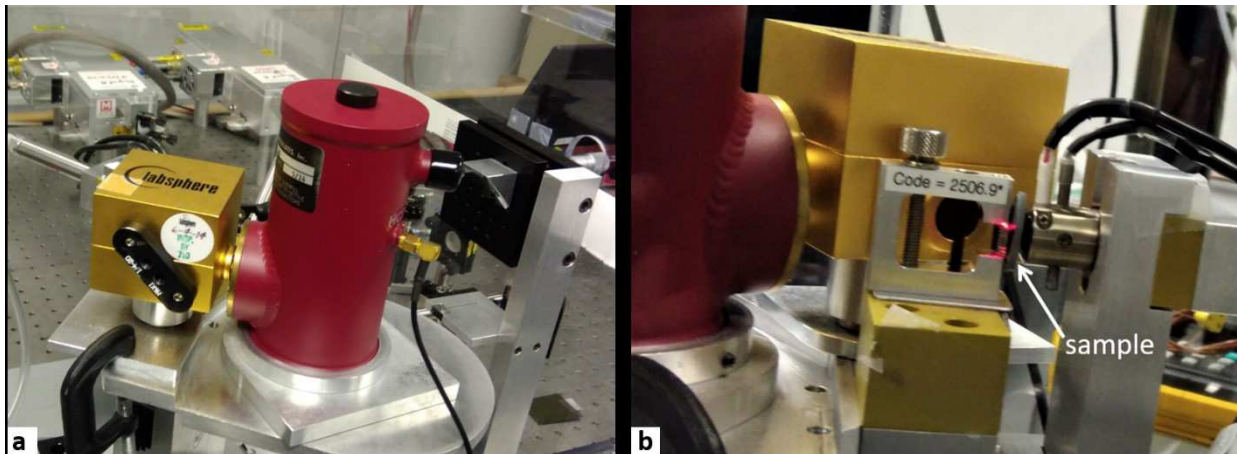


Figure 4.7. Metricon Model 2010/M Prism Coupler utilized for the refractive index measurement (a). The sample is placed between the prism and the coupling head (b).

An adequate piece was retrieved from leftovers of the drawing of first tube (Figure 3.3). Since it was already smooth and flat enough, no polishing was needed (Figure 4.8).



Figure 4.8. Image of tellurite glass sample used for the refractive index measurement. Each mark of the ruler stands for 1 mm.

The measurement was performed at a wavelength of 0.98 μm . It was carried out at room temperature and repeated 10 times in order to calculate mean value and standard deviation. The result is illustrated in Table 4.2.

Tab 4.2. Outcome of the refractive index measurement on TZN glass sample, carried out at a wavelength of 0.98 μm . Refractive index value is reported for each calculation, along with mean value and standard deviation.

<i>Sequence</i>	<i>GaP Prism</i>	<i>TZN Sample</i>
1	3.1238	2.0011
2	3.1241	2.0009
3	3.1241	2.0007
4	3.1239	2.0009
5	3.1240	2.0007
6	3.1239	2.0004
7	3.1242	2.0010
8	3.1241	2.0012
9	3.1240	2.0007
10	3.1239	2.0007
Mean value	3.1240	2.0008
Standard deviation	0.0001	0.0002

As can be seen, the final outcome gave a refractive index of 2.0008. Although it was measured only at 0.98 μm , it is well known that, with regard to TZN glasses, normally its value slightly decreases at higher wavelengths. Thus, this aspect must be taken into account in view of future applications.

4.3 FTIR Spectroscopy

Spectroscopy measurements allow to analyze the interaction between matter and electromagnetic radiations. Since their appearance, they have been essential in almost every branch of science and technology, leading to significant discoveries and breakthroughs.

To date, many techniques have been built, each one with unique features that let study specific characteristics of materials and the physical world in general. Among others, *infrared spectroscopy* is widely used in materials science, especially to determine absorption spectra and structural units.

Infrared radiation has less energy than visible light, since it is characterized by longer wavelengths that go from 0.7 μm to 1 mm. Its interaction with matter provokes perturbation of the dipole moment of molecules, inducing molecular vibrations and rotations whenever photons of those frequencies are absorbed. Since each chemical bond vibration is different and belongs to a specific frequency, the analysis of IR absorption allows to identify unknown compounds and control chemical reactions. Additionally, another accessory application commonly used consists in verifying the purity of a given sample, since undesired molecules (such as OH groups in optical fibers) might be present. In fiber optics, moreover, a special importance is given to the study of the transmittance of materials designed to guide light in that range of the electromagnetic spectrum.

Among the techniques available, the *FTIR (Fourier Transform Infrared) spectrometer* is frequently utilized in research. Its main advantage compared to dispersive equipment is the ability to gather all wavelengths at the same time. Indeed, rather than working with monochromatic light, it makes use of a beam that simultaneously contains the entire range of wavelengths to be measured. Whenever data concerning the amount of light absorbed by the specimen is collected, the beam is altered and another measurement of absorption, at a different combination of frequencies, is made. This procedure is iterated and, when all data is obtained, it is processed by a computer that extracts the transmission spectrum performing a Fourier Transform.

Therefore, this method was employed on the TZN glass with the intention of identifying its optimal transmission window and verify the presence and quantity of OH absorption typical of the mid-IR range. A Thermo Scientific Nicolet iS5 FTIR Spectrometer was employed to measure the infrared transmittance spectrum in the range from 400 to 7000 cm^{-1} (Figure 4.9). The sample used was the same utilized for the hardness test (Figure 4.4). It was 1.8 mm thick and polished both sides to an optical quality.



Figure 4.9. Thermo Scientific Nicolet iS5 FTIR Spectrometer utilized for the FTIR analysis.

For each wavelength of interest, the instrumentation analyzes the transmittance, defined as:

$$T = I/I_0, \quad (4.7)$$

where I_0 is the initial light intensity and I is the intensity of light detected after its passage across the sample.

The output obtained is shown in Figure 4.10. A broader graph containing the whole spectrum from 1.4 μm to 25 μm is presented in Appendix 6.3.

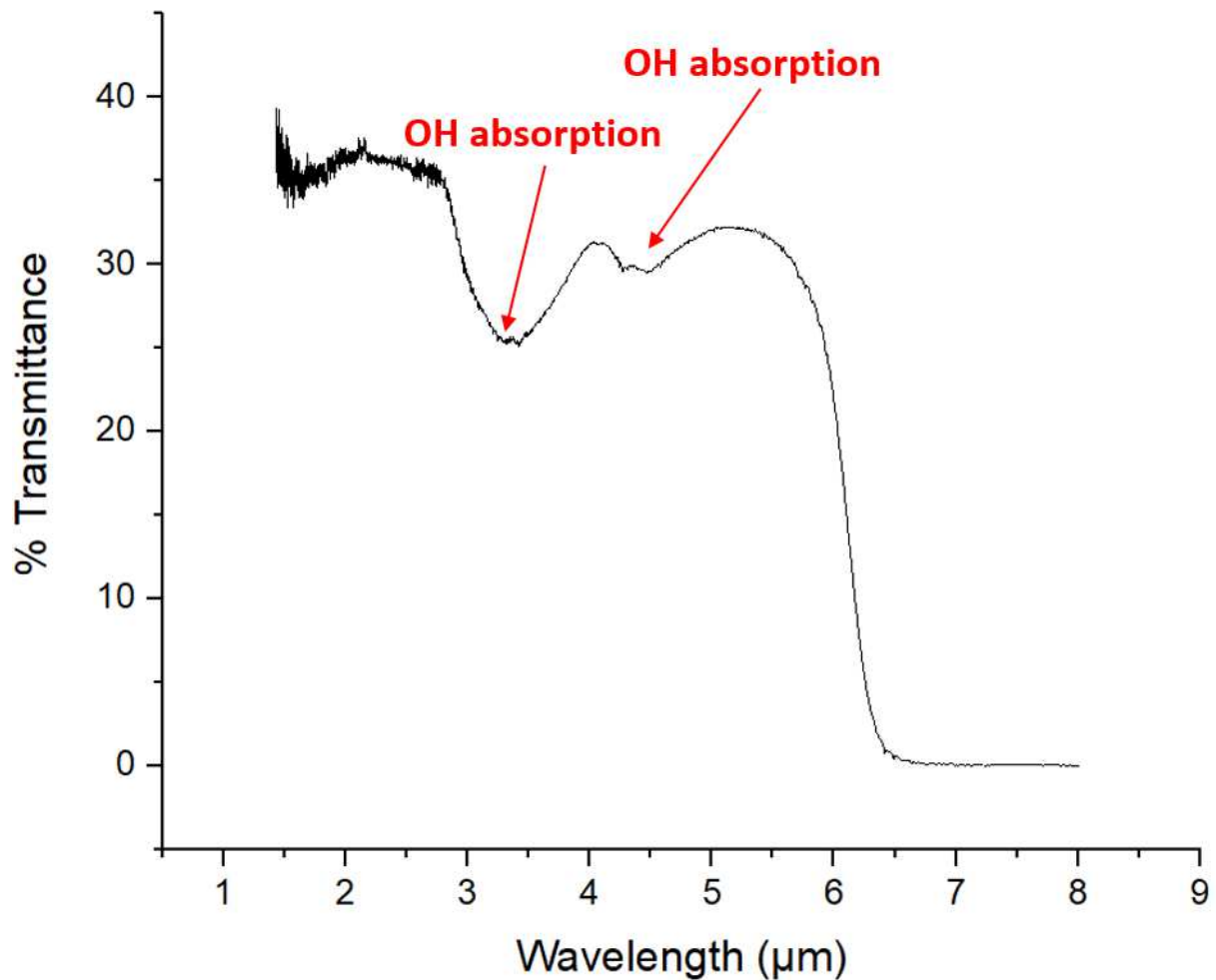


Figure 4.10. FTIR spectrum of TZN glass in the range of wavelengths between 1.4 μm and 8 μm , with corresponding peaks of OH absorption at around 3.3 μm and 4.4 μm . Thickness of the tested sample was 1.8 mm.

The result reflects what expected from literature in terms of transmission window, which is fairly broad and up to nearly 6 μm , although minimum losses are just until 2.8 μm . Nevertheless, there are two peaks of absorption at around 3.3 μm and 4.4 μm respectively, which are attributed to the vibration of OH impurities. Specifically, the first and deeper concavity of the curve is supposed to be caused by a combination of weakly H-bonded OH and free OH, while the second by strongly H-bonded OH groups [33].

Presumably, hydroxyl groups were not completely removed from bulk glass during the synthesis. Further improvements on tubes fabrication could enhance the result, though it is well known how difficult it is to avoid any form of impurity.

In any case, the OH absorption leads to a transmission decrease lower than 10%, which might be acceptable considering that, for tellurite glasses, this impurity is the most damaging in the 2-5 μm range.

4.4 Results and discussion

All the samples used for the measurements were acquired from the drawing of first tube (Figure 3.3). Specifically, leftovers of suitable sizes were collected and then processed to fulfill the requirements of each instrument.

The values obtained for different physical properties of TZN, either measured directly on glass samples or extrapolated from literature, are summarized in Table 4.1.

Table 4.3. Physical properties values of TZN glass, including chemical composition, glass transition temperature T_g , crystallization onset temperature $T_{x,onset}$, thermal stability ΔT , coefficient of thermal expansion α , viscosity η , Vickers microhardness HV, refractive index n at 0.98 μm .

Chemical Composition (molar %)	75%TeO ₂ -15%ZnO-10%Na ₂ O
$T_g \pm 2 \text{ }^\circ\text{C}$	283 $^\circ\text{C}$
$T_{x,onset} \pm 2 \text{ }^\circ\text{C}$	407 $^\circ\text{C}$
ΔT	124 $^\circ\text{C}$
α (25 $^\circ\text{C}$ - 250 $^\circ\text{C}$)	$18.8 \times 10^{-6} \text{ }^\circ\text{C}$
Vickers microhardness $\pm 9 \text{ HV}$	323 HV
n at 0.98 $\mu\text{m} \pm 0.0002$	2.0008

From DSC, an adequate stability against devitrification emerged. This allows to carry out fiber drawing processes with no concern about any eventual crystallization event.

Because of the lack of an appropriate specimen and the impossibility of making one, the CTE was acquired from literature and not experimentally. It is always important to know it, albeit in this specific case was not crucial for fiber fabrication since core and cladding were identical materials.

The same applies to viscosity, with the difference that in this case it was not possible to obtain accurate results from other publications. Only a few values belonging to a similar composition were found. Since viscosity is very important especially for fiber drawing, a direct measurement of it would be very useful. Then, the result should be the perfect starting point for the individuation of the right drawing temperature, accompanied by the experience gained empirically during previous drawings.

Hardness test confirmed the brittleness of this material, which is highly inclined to get damaged at the minimum stress applied. It would be interesting to study how hardness varies with small changes of chemical composition.

To measure the refractive index was chosen the prism coupling technique. The result was as expected, although it refers to only one wavelength (0.98 μm). It would be helpful to repeat the measurement using different laser sources and find out how the refractive index varies with wavelength.

Since the transmission window turned out to be wide and has the best values up to almost 3 μm , there is a good chance that a TZN fiber could be successfully tested as supercontinuum source. Further improvement in the reduction of OH content could allow to extend supercontinuum generation, theoretically up to 6 μm .

With the purpose of augmenting even more the pureness of the glass, a slight modification of the chemical composition may be a doable option. For instance, the addition of halogen-containing compounds such as sodium chloride (NaCl) and barium chloride (BaCl₂) could reduce the OH content through pyrohydrolysis reactions [9]:



All this could permit to extend the window of minimum losses beyond 3 μm .

5 Conclusions

Tellurite glasses have several features that reveal the possibility to carry out remarkable fundamental research and technological development. In this work it has been presented an overview of their peculiar properties, giving special attention to optical and thermomechanical behaviors.

Characterization made it possible to analyze the TZN glass of the composition selected. Differential scanning calorimetry, hardness, prism coupling method and FTIR spectroscopy were performed on samples retrieved from the drawing of the first tube. Furthermore, the research of selected publications permitted to deduce plausible values for viscosity and coefficient of thermal expansion.

A great deal of the work was entirely dedicated to designing and fabricating a TZN photonic crystal fiber via stack-and-draw technique. The unexpected negative outcome of fiber drawing precluded the possibility of obtaining and characterizing such PCF, turning the focus on the examination of the causes of the failure. An analysis of possible alternative strategies for future activities in that direction was made, too.

Overall, the experimental activity conducted was also useful to acquire experience in handling this material so different from silica. This aspect can make a difference if another attempt to fabricate TZN fibers will be made.

6 Appendix

6.1 CVD and materials used

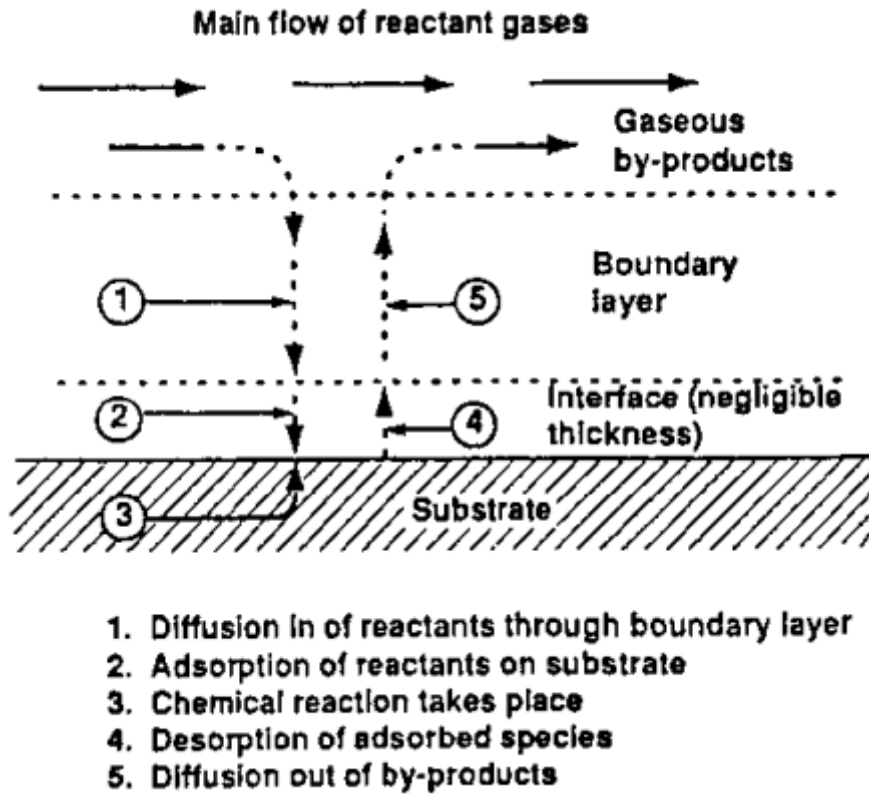


Figure 6.1. Sequence of steps that occur during deposition (figure retrieved from [19]).

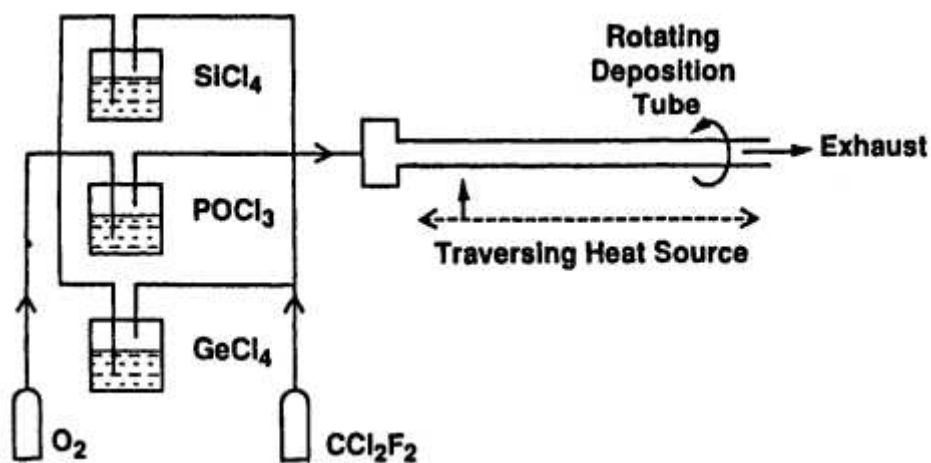


Figure 6.2. Schematic of chemical deposition technology for optical fibers (figure retrieved from [19]).

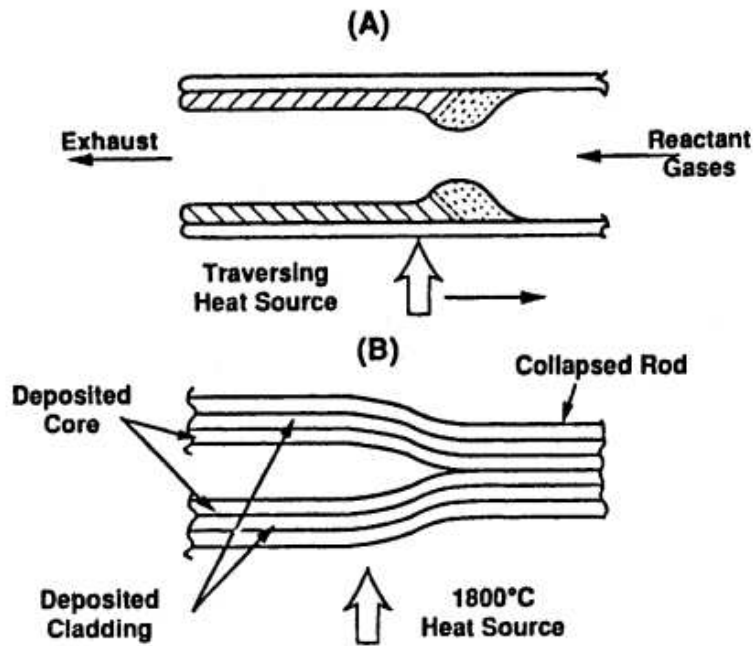


Figure 6.3. Representation of cladding deposition (A) and tube collapse (B) in fiber optics production (figure retrieved from [19]).

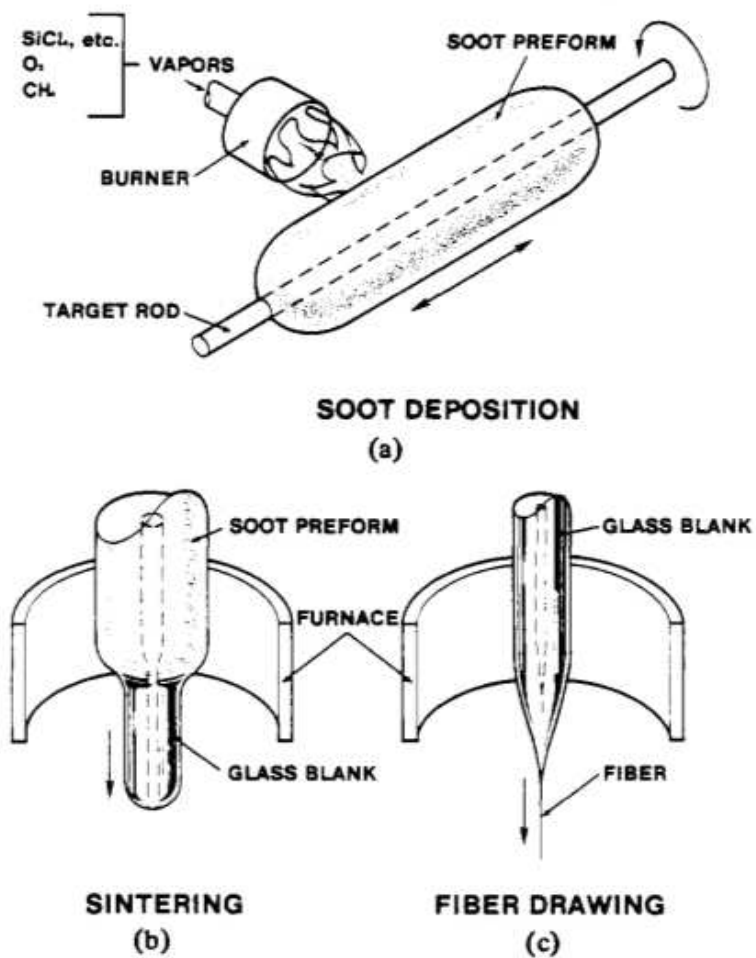


Figure 6.4. Schematic of the OVD process for fiber production: soot deposition on a target rod (a), preform sintering (b) and fiber drawing from the glass blank (c) (figure retrieved from [21]).

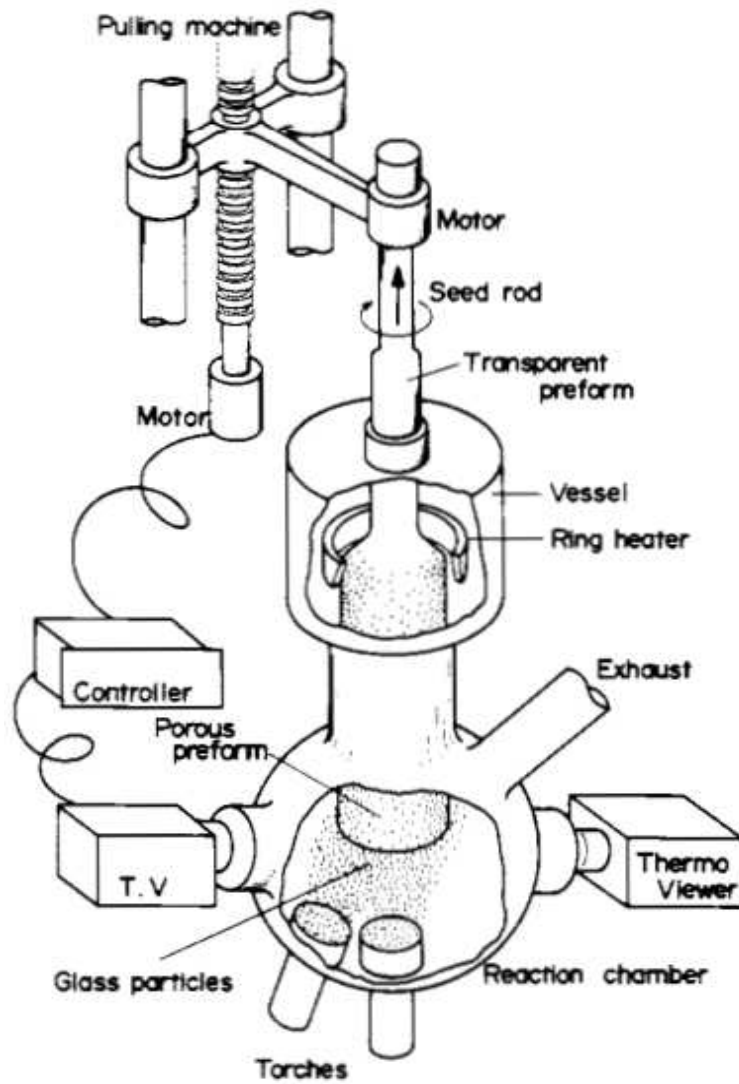


Figure 6.5. Equipment for VAD process (figure retrieved from [22]).

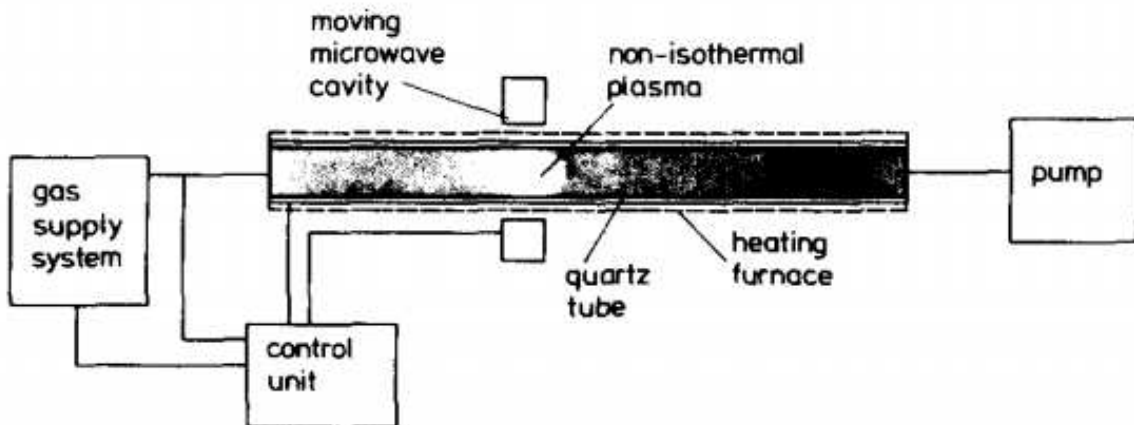


Figure 6.6. Schematic view of the PCVD apparatus (figure retrieved from [23]).

Table 6.1. Some properties of typical halides used in CVD; (s) indicates that the compound sublimes at atmospheric pressure before melting [19].

<i>Halides</i>	<i>Melting point °C</i>	<i>Boiling point °C</i>
AlBr ₃	97.5	263
AlCl ₃	190	182.7 (s)
BCl ₃	-107.3	12.5
BF ₃	126.7	-99.9
CCl ₄	-23	76.8
CF ₄	-184	-128
CrCl ₂	824	1300 (s)
NbCl ₅	204.7	254
SiCl ₄	-70	57.6
TiCl ₄	-25	136
VCl ₄	-28	148.5
WCl ₅	248	275.6
ZrCl ₄	437	331 (s)
ZrBr ₄	450	357 (s)

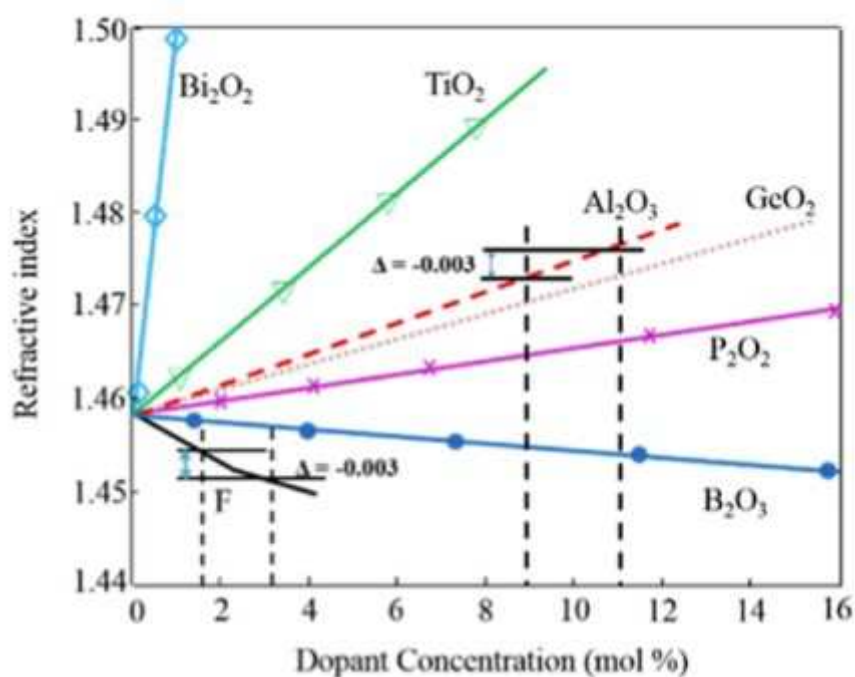


Figure 6.7. Variation of silica's refractive index as a function of dopant concentration for Bi₂O₂, TiO₂, Al₂O₃, GeO₂, P₂O₂, B₂O₃ and F (figure retrieved from [34]).

6.2 DSC curve

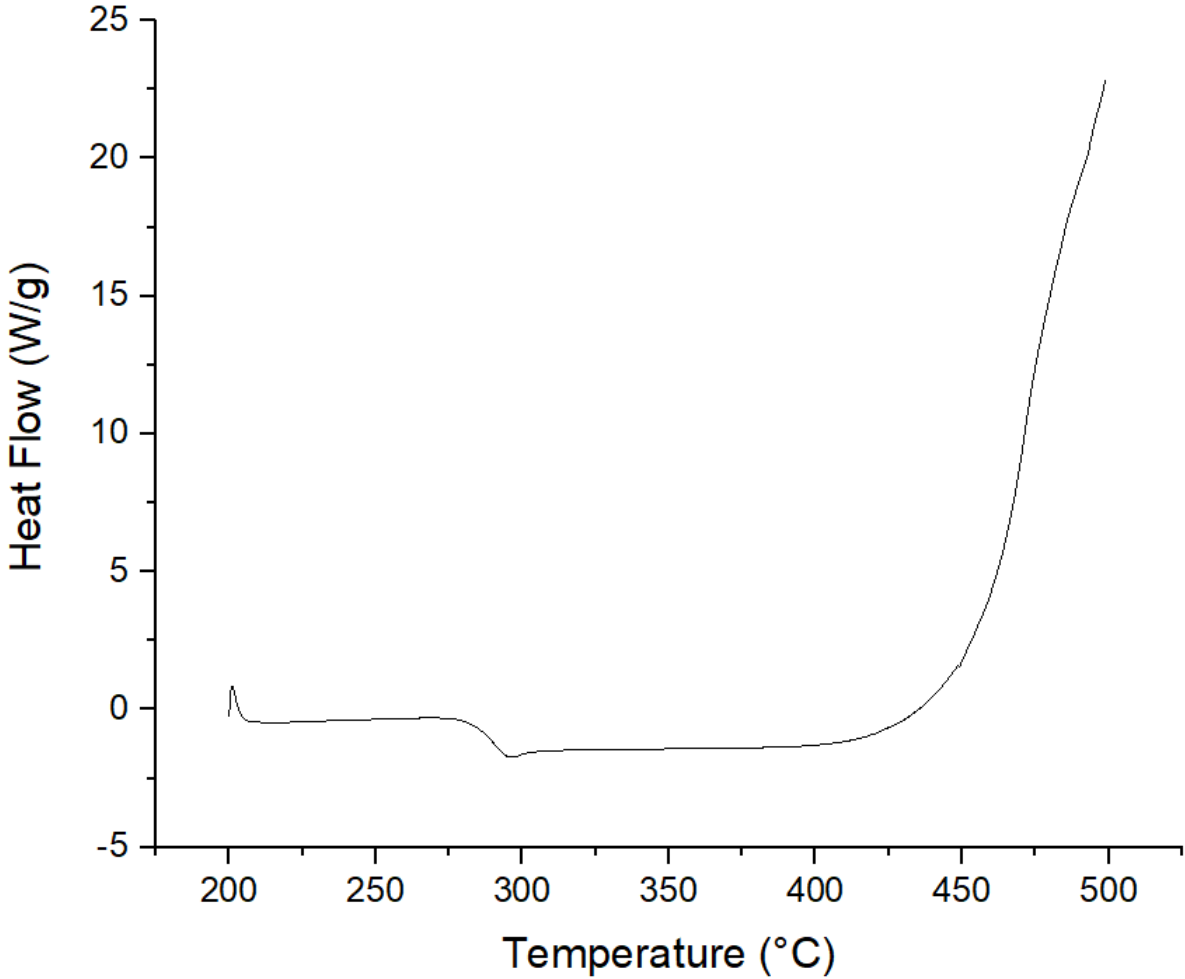


Figure 6.8. DSC spectra of TZN glass from 200 °C to 500 °C. Exothermic reactions are shown with a positive peak.

6.3 FTIR spectrum

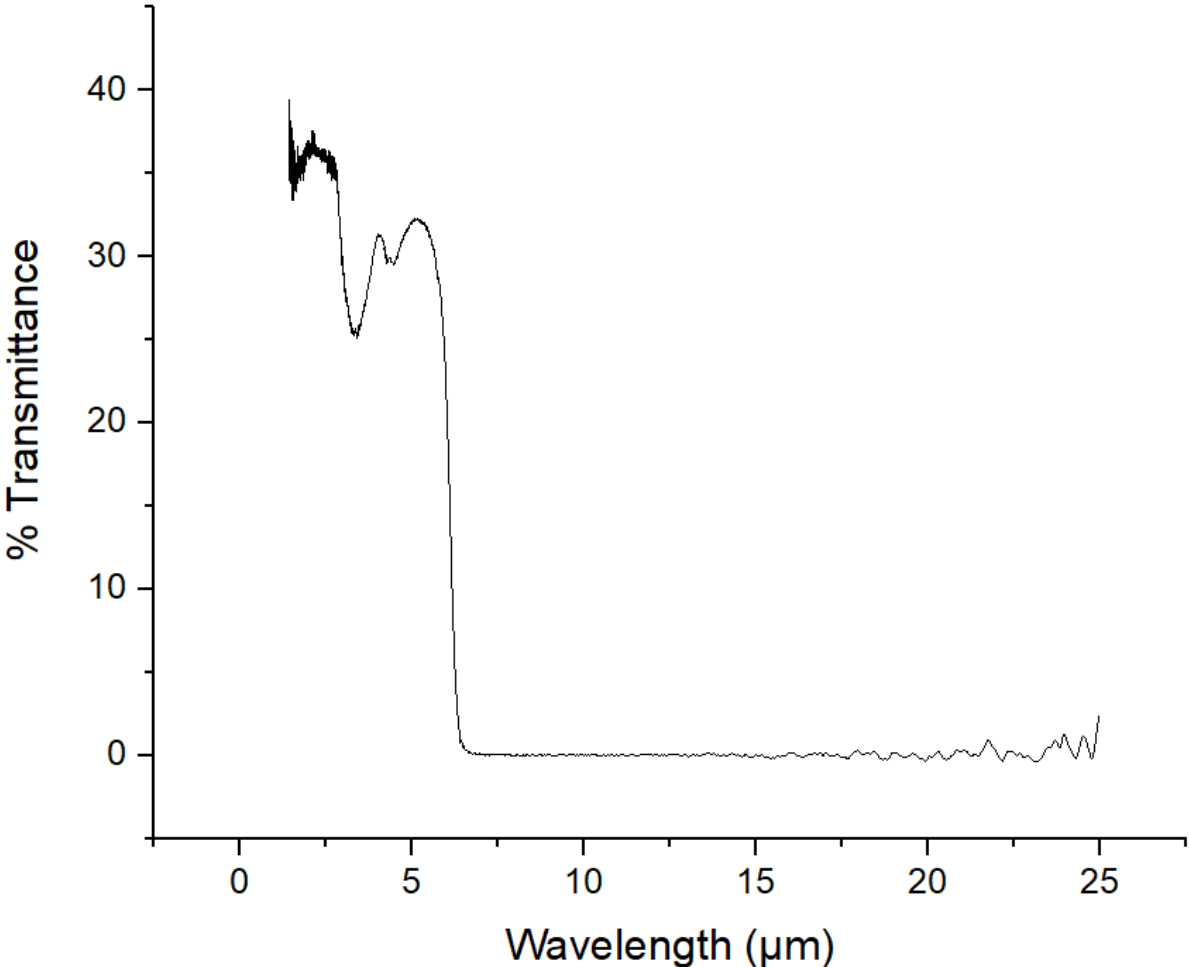


Figure 6.9. FTIR spectrum of TZN glass in the range of wavelengths between 1.4 μm and 25 μm. Thickness of the tested sample is 1.8 mm.

7 List of symbols and abbreviations

TIR	Total Internal Reflection
OVPO	Outside Vapor Phase Oxidation
POF	Polymer Optical Fibers
PMMA	Poly(methyl methacrylate)
PCF	Photonic Crystal Fiber
SEM	Scanning Electron Microscope
IR	Infrared
MIR	Mid-Infrared
VIS	Visible
MOF	Microstructured Optical Fiber
tbp	Trigonal bi-pyramid
tp	Trigonal pyramid
n	Linear refractive index
TZN	TeO ₂ -ZnO-Na ₂ O
CTE	Coefficient of thermal expansion
T _g	Glass transition temperature
T _x	Crystallization temperature
CVD	Chemical Vapor Deposition
MCVD	Modified Chemical Vapor Deposition
OVD	Outside vapor deposition
VAD	Vapor phase axial deposition
PCVD	Plasma chemical vapor deposition
UV	Ultraviolet
OM	Optical Microscope
OD	Outer diameter
ID	Inner diameter
PTFE	Polytetrafluoroethylene
DSC	Differential scanning calorimetry
η	Viscosity
α	Linear coefficient of thermal expansion
TMA	Thermomechanical analysis
LVDT	Linear variable differential transformer

HV

Vickers hardness

FTIR

Fourier Transform Infrared

References

- [1] Buck J. A., 2004, *Fundamentals of Optical Fibers*. Wiley-Interscience. [ISBN 0-471-22191-0]
- [2] Lee B., 2003, Review of the present status of optical fiber sensors. *Optical fiber technology*, **9**, 57-79. [DOI: 10.1016/S1068-5200(02)00527-8]
- [3] Hecht J., 2004, *City of Light, The Story of Fiber Optics*. Oxford University Press. [ISBN 9780195162554]
- [4] Crisp J., Elliott B., 2005, *Introduction to fiber optics*. Elsevier. [ISBN 978-0-7506-6756-2]
- [5] Mangan B. J., Farr L., Langford et al., 2004, Low loss (1.7 dB/km) hollow core photonic bandgap fiber. *IEEE*. [ISBN 1-55752-772-5]
- [6] Pysz D., Kujawa I., Stepień R., Klimczak M., Filipkowski A., Franczyk M., Kociszewski L., Buzniak J., Harasny K., Buczynski R., 2014, Stack and draw fabrication of soft glass microstructured fiber optics. *Bulletin of the Polish academy of sciences technical sciences*, **62 (4)**. [DOI: 10.2478/bpasts-2014-0073]
- [7] Toulouse J., Lin A., Ryznyanskiy A., Belwalkar A., Guintrand C., Lafontaine C., Misiolek W., Biaggio I., 2011, Development of New Tellurite Fibers for mid-IR Applications. *IEEE*. [DOI: 10.1109/PHOTWMTM.2011.5730109]
- [8] Tao G., Ebendorff-Heidepriem H., Stolyarov A. M., Danto S. et al., 2015, Infrared Fibers. *Advances in Optics and Photonics*, **7**, 379-458. [DOI: 10.1364/AOP.7.000379]
- [9] Rivera V. A. G., Manzani D., 2017, *Technological Advances in Tellurite Glasses*. Springer. [ISBN 978-3-319-53036-9]
- [10] T. Sekiya, N. Mochida, A. Ohtsuka, M. Tonokawa, 1989, Normal vibrations of two polymorphic forms of TeO₂ crystals and assignment of raman peaks of pure TeO₂ glass. *Nippon Seramikkusu Kyokai Gakujutsu Ronbunshi*, **97(12)**, 1435-1440. [DOI: 10.2109/jcersj.97.1435]
- [11] Jha A., Richards B. D. O., Jose G., Toney Fernandez T., Hill C. J., Lousteau J., Joshi P., 2012, Review on structural, thermal, optical and spectroscopic properties of tellurium oxide based glasses for fibre optic and waveguide applications. *International Materials Reviews*, **57(6)**, 357-382. [DOI: 10.1179/1743280412Y.0000000005]
- [12] Tong L., Hu L., Zhang J., Qiu J., Yang Q., Lou J., Shen Y., He J., Ye Z., 2006, Photonic nanowires directly drawn from bulk glasses. *Optics Express*, **14(1)**, 82-87. [DOI: 10.1364/OPEX.14.00008]
- [13] Rivera V. A. G., Chilloce E.F., Rodriguez E., Cesar C.L., Barbosa L.C., 2006, Planar waveguides by ion exchange in Er³⁺-doped tellurite glass. *Journal of Non-Crystalline Solids*, **352 (5)**, 363-367. [DOI: 10.1016/j.jnoncrysol.2006.01.018]
- [14] Liao M., Gao W., Duan Z., Yan X., Suzuki T., Ohishi Y., 2012, Supercontinuum generation in short tellurite microstructured fibers pumped by a quasi-cw laser. *Optics Letters*, **37(11)**, 2127-2129. [DOI: 10.1364/OL.37.002127]

- [15] Delmonte T., Warson M. A., O'Driscoll E. J., Feng X., Monro T. M., Finazzi V., Petropoulos P., Price J. H. V., Baggett J. C., Loh W., Richardson D. J., Hand D. P., 2006, Generation of mid-IR continuum using tellurite microstructured fiber. *Conference on Lasers and Electro-Optics/Quantum Electronics and Laser Science Conference and Photonic Applications Systems Technologies*, Long Beach, California, USA, 21-26 May 2006
- [16] Paschotta R., 2008, *Encyclopedia of Laser Physics and Technology*. Wiley-VCH, Berlin. [ISBN 978-3-527-40828-3]
- [17] Chen Q., Wang H., Wang Q., Chen Q., Hao Y., 2015, Modified rod-in-tube for high-NA tellurite glass fiber fabrication: materials and technologies. *Applied Optics*, **54(4)**, 946-952. [DOI: 10.1364/AO.54.000946]
- [18] Nagel S. R., MacChesney J. B., Walker K. L., 1982, An Overview of the Modified Chemical Vapor Deposition (MCVD) Process and Performance. *IEEE Transactions on Microwave Theory and Techniques*, **30(4)**, 305-322. [DOI: 10.1109/TMTT.1982.1131071]
- [19] Pierson H. O., 1999, *Handbook of Chemical Vapor Deposition (CVD)*. Noyes publications, Park Ridge, New Jersey. [ISBN 978-0-8155-1432-9]
- [20] Yang J., 2008, Numerical modelling of hollow optical fiber drawing process. Ph.D. dissertation, Rutgers University, New Brunswick, New Jersey.
- [21] Schultz P. C., 1980, Fabrication of Optical Waveguides by the Outside Vapor Deposition Process. *Proceedings of the IEEE*, **68(10)**, 1187-1190. [DOI: 10.1109/PROC.1980.11828]
- [22] Izawa T., Inagaki N., 1980, Materials and Processes for Fiber Preform Fabrication - Vapor Phase Axial Deposition. *Proceedings of the IEEE*, **68(10)**, 1184-1187. [DOI: 10.1109/PROC.1980.11827]
- [23] Geittner P., Küppers D., Lydtin H., 2008, Low-loss optical fibers prepared by plasma-activated chemical vapor deposition (CVD). *Applied Physics Letters*, **28**, 645. [DOI: 10.1063/1.88608]
- [24] Russell P., 2003, Photonic Crystal Fibers. *Science*, **299(5605)**, 358-362. [DOI: 10.1126/science.1079280]
- [25] Hidnert P., Krider H. S., 1952, Thermal Expansion of Aluminum and Some Aluminum Alloys. *Journal of Research of the National Bureau of Standards*, **48(3)**.
- [26] Manning S., Ebandorff-Heidepriem H., Monro T., 2012, Ternary tellurite glasses for the fabrication of nonlinear optical fibers. *Optical Materials Express*, **2(2)**, 140-152. [DOI: 10.1364/OME.2.000140]
- [27] ASTM International, 2002, C 1351M-96. Standard Test Method for Measurement of Viscosity of Glass Between 10^4 Pa·s and 10^8 Pa·s by Viscous Compression of a Solid Right Cylinder.
- [28] Animesh Jha, 2016, *Inorganic Glasses for Photonics Fundamentals, Engineering, and Applications*. Wiley. [ISBN 9781118696088]
- [29] Lin A., Zhang A., Bushong E. J., Toulouse J., 2009, Solid-core tellurite glass fiber for infrared and nonlinear applications. *Optics Express*, **17(19)**, 16716-16721. [DOI: 10.1364/OE.17.016716]

- [30] Takeuchi Y., Mitachi S., 1997, High-Strength Glass–Ceramic Ferrule for SC-Type Single-Mode Optical Fiber Connector. *IEEE Photonics Technology Letters*, **9(11)**, 1502-1504. [DOI: 10.1109/68.634722]
- [31] Wilantewicz T. E., Varner J. R., Vickers indentation behavior of several commercial glasses at high temperatures. *Journal of Materials Science*, **43(1)**, 281-298. [DOI: 10.1007/s10853-007-2174-9]
- [32] Onodera H., Awai I., Ikenoue J., 1983, Refractive-index measurement of bulk materials: prism coupling method. *Applied Optics*, **22(8)**, 1194-1197. [DOI: 10.1364/AO.22.001194]
- [33] Savellii I., Desevedavy F., Jules J., Gadret G., Fatome J. et al., 2013, Management of OH absorption in tellurite optical fibers and related supercontinuum generation. *Optical Materials*, **35(8)**, 1595-1599. [DOI: 10.1016/j.optmat.2013.04.012]
- [34] Muhammad A. R., Emami S. D., Hmood J. K., Sayar K., Penny R., Abdul-Rashid H. A., Ahmad H. and Harun S. W., 2014, Enhanced Performance of an S-Band Fiber Laser using Thulium doped Photonic Crystal Fiber. *Laser Physics*, **24**, 11. [DOI: 10.1088/1054-660X/24/11/115201]